

A Comparison of Semi-Analytic and Smoothed Particle Hydrodynamics Galaxy Formation

A. J. Benson^{1,2}, F. R. Pearce¹, C. S. Frenk¹, C. M. Baugh¹ and A. Jenkins¹

1. *Physics Department, University of Durham, Durham DH1 3LE, England.*

2. *E-mail: A.J.Benson@dur.ac.uk*

11 November 2021

ABSTRACT

We compare the statistical properties of galaxies found in two different models of hierarchical galaxy formation: the semi-analytic model of Cole et al. and the smoothed particle hydrodynamics (SPH) simulations of Pearce et al. These two techniques model gas processes very differently: by approximate, analytic methods in the case of the semi-analytic model, and by direct numerical integration of the equations of hydrodynamics for a set of discrete particles in the case of SPH. Using a ‘stripped-down’ version of the semi-analytic model which mimics the resolution of the SPH simulations and excludes physical processes not included in them, we find that the two models produce an ensemble of galaxies with remarkably similar properties, although there are some differences in the gas cooling rates and in the number of galaxies that populate halos of different mass. The full semi-analytic model, which has effectively no resolution limit and includes a treatment of star formation and supernovae feedback, produces somewhat different (but readily understandable) results. Our comparison demonstrates that, on the whole, SPH simulations and semi-analytic models give similar results for the thermodynamic evolution of cooling gas in cosmological volumes. Agreement is particularly good for the present-day global fractions of hot gas, cold dense (i.e. galactic) gas and uncollapsed gas, for which the SPH and stripped-down semi-analytic calculations differ by at most 25%. In the most massive halos, the stripped-down semi-analytic model predicts, on the whole, up to 50% less gas in galaxies than is seen in the SPH simulations. The two techniques apportion this cold gas somewhat differently amongst galaxies in a given halo. This difference can be tracked down to the greater cooling rate in massive halos in the SPH simulation compared to the semi-analytic model. The galaxy correlation functions in the two models agree to better than about 50% over most pair separations and evolve with redshift in very similar ways. Our comparison demonstrates that these different techniques for modelling galaxy formation produce results that are broadly consistent with each other and highlights areas where further study is required.

Key words: methods: numerical - galaxies: formation: kinematics and dynamics - cosmology: theory - hydrodynamical simulation

1 INTRODUCTION

The properties of galaxies in the Universe are determined by the behaviour of both the dark matter and the baryonic material from which they are made. The dynamics of the dark matter, which are determined by gravity alone, are now reasonably well understood. N-body simulations (e.g. Davis et al. 1985) provide an accurate description of the evolution of structure into the highly non-linear regime where dark matter halos form (see, for example Jenkins et al. 1998; Colin et al. 1999). Analytically, the Press-Schechter theory (Press &

Schechter 1974) predicts to within $\sim 50\%$ the distribution of halo masses found in N-body simulations for a specified cosmology, whilst theoretically motivated fitting functions do even better (Sheth & Tormen 1999; Sheth, Mo & Tormen 1999; Jenkins et al. 2000). Extensions of this theory (Bond et al. 1991; Bower 1991; Lacey & Cole 1993) predict, with reasonable accuracy, the hierarchical build-up of halos through the mergers of smaller progenitors (see, for example, Lacey & Cole 1994; Somerville et al. 2000). The behaviour of the baryonic matter, on the other hand, is less well understood. The dynamics of the gas are not determined by

gravity alone but also by hydrodynamical forces and radiative processes. Since gas must cool into dense lumps before it can turn into stars, these processes are crucial for galaxy formation (see, for example, Binney 1977; Rees & Ostriker 1977; Silk 1977; White & Rees 1978).

In this paper, we compare the outcome of two widely used techniques for modelling the behaviour of gas as it forms into galaxies: semi-analytic modelling and direct simulation using smoothed particle hydrodynamics (SPH). Semi-analytic models applied to cold dark matter (CDM) cosmologies (Cole 1991; White & Frenk 1991; Lacey & Silk 1991; Kauffmann, White & Guiderdoni 1993; Cole et al. 1994; Somerville & Primack 1999; Cole et al. 2000) have met with considerable success in explaining many of the observed properties of the galaxy population, such as the luminosity function, the distributions of colour and morphological type, the counts as a function of magnitude and redshift (e.g. White & Frenk 1991; Lacey et al. 1993; Kauffmann, Guiderdoni & White 1994; Cole et al. 1994; Kauffmann 1995; Baugh, Cole & Frenk 1996a,b; Kauffmann 1996a,b; Kauffmann & Charlot 1998a,b), the properties of Lyman-break galaxies (Baugh, Cole, Frenk & Lacey 1998; Governato et al. 1998), and the clustering of galaxies (Kauffmann, Nusser & Steinmetz 1997; Kauffmann et al. 1999a,b; Diaferio et al. 1999; Baugh et al. 1999; Benson et al. 2000a,b).

The SPH technique (Lucy 1977; Gingold & Monaghan 1977) has been used by many authors to model galaxy formation (e.g. Katz & Gunn 1991; Katz, Hernquist & Weinberg 1992; Navarro & White 1993; Evrard, Summers & Davis 1994; Steinmetz & Müller 1995,1996; Katz, Weinberg & Hernquist 1996; Frenk et al. 1996; Weil, Eke & Efstathiou 1998; Navarro & Steinmetz 1999; Pearce et al. 1999). These simulations have been successful in producing objects with approximately the mass of galaxies and, in cosmological simulations, with approximately the right abundance. However, to date no simulation has been able to produce a realistic, rapidly rotating spiral galaxy starting from cosmological initial conditions (e.g. Navarro & Steinmetz 1999).

Both techniques require a number of simplifying assumptions in order to model the evolution of cooling gas. For example, semi-analytic models assume that dark matter halos and their associated gas component are spherically symmetric, and that gas is efficiently shock-heated when halos collapse. SPH, on the other hand, assumes that gas is well represented by a set of discrete particles. The two methods have different strengths and limitations. Semi-analytic modelling can follow a large dynamic range of scales and is sufficiently flexible that the effects of varying assumptions and parameter values can be readily explored. SPH, on the other hand, does not impose any restrictions on geometry and solves directly the approximate evolution equations for gravitationally coupled dark matter and dissipative gas. Limited resolution, however, restricts the accessible dynamic range and the expense of large simulations makes it impractical to carry out extensive parameter space explorations. In both approaches, a phenomenological model for star formation and feedback must be coupled to the evolution of dark matter and gas in order to calculate observable properties of galaxies. Generally, such models are more easily implemented in semi-analytic models than in SPH simulations in

which the behaviour of the phenomenological model itself often depends on resolution.

The main aim of this paper is to determine the extent to which the two techniques of semi-analytic modelling and SPH simulation produce consistent results for the evolution of cooling gas in the cosmological setting relevant to galaxy formation. There are several ways in which such a comparison might be carried out. In this paper, we adopt the statistical approach of comparing the properties of *populations* rather than of individual objects. This comparison is motivated by two considerations. Firstly, we wish to understand how the different approximations inherent in the two techniques translate into differences in the *average* properties of the two models. Secondly, both techniques have been used (and continue to be used) to study statistical properties such as galaxy luminosity functions and spatial correlation functions. It is clearly important to test how reproducible these bulk properties are using these rather different modelling techniques. A complementary approach, which we defer to a later paper, is to compare the properties of individual objects modelled using the two techniques. A secondary aim of our paper is to assess how the neglect of sub-resolution processes in SPH simulations, i.e. star formation and feedback, can affect the properties of objects above the resolution limit.

When differences between the results of the two modelling techniques do arise, it is difficult to know which of the two, if either, is giving the “correct” answer. In some cases, however, we can explore the reasons for a disagreement by altering parameters in the semi-analytic model which describe a specific physical process, for example, the galaxy merger timescale. In this way, we can identify specific areas of disagreement in which further theoretical work is required.

This paper is laid out as follows. In §2, we briefly describe the SPH and semi-analytic models, and discuss in greater detail their specific implementation in this work. In §3, we compare several properties of the galaxies calculated using the two techniques, and uncover the reasons for some of the differences by varying key parameters in the semi-analytic models. Finally, in §4, we present our conclusions.

2 THE SPH SIMULATIONS AND SEMI-ANALYTIC MODELS

We now present the models of galaxy formation employed in this paper. Since the SPH and semi-analytic techniques are described in detail elsewhere, we give only a brief overview here, referring the reader to the appropriate references for further details where applicable.

2.1 SPH Simulations

2.1.1 Techniques

The SPH technique is a Lagrangian method in which the gaseous component of the universe is described by a set of tracer gas elements represented by particles within the simulation volume. Estimates of local gas properties (and their spatial derivatives) for each particle are derived by smoothing over the properties of the N_{SPH} nearest neighbour particles (see Monaghan (1992) for a review). For simulations

of galaxy formation, the gas must also be able to cool radiatively.

The simulation volume is initially populated with dark matter and gas particles, with a spatial distribution derived from a cosmological power spectrum. The equations of gravity and hydrodynamics are then solved over a succession of small timesteps in order to propagate the particle distribution forwards in time until the present day.

2.1.2 Simulation Specifics

Simulations were carried out for two of the cold dark matter cosmological models studied by Jenkins et al. (1998): Λ CDM (mean mass density parameter, $\Omega_0 = 0.3$; cosmological constant, in units of $3H_0^2/c^2$, $\Lambda_0 = 0.7$; Hubble constant, in units of $100 \text{ km s}^{-1} \text{ Mpc}^{-1}$, $h = 0.7$; and rms linear fluctuation amplitude in $8h^{-1} \text{ Mpc}$ spheres, $\sigma_8 = 0.9$), and SCDM ($\Omega_0 = 1.0$, $\Lambda_0 = 0$, $h = 0.5$, $\sigma_8 = 0.6$). The baryon fraction in each cosmology was set, from nucleosynthesis constraints, to be $\Omega_b h^2 = 0.015$ (Copi, Schramm & Turner 1995). The simulations, which were carried out using the parallel AP3M-SPH code of Pearce & Couchman (1997), have 128^3 particles of each species in boxes of side $70h^{-1} \text{ Mpc}$ and $50h^{-1} \text{ Mpc}$ in the Λ CDM and SCDM models respectively. The gas mass per particle is therefore 1.4×10^9 and $1.0 \times 10^9 h^{-1} M_\odot$ in the Λ CDM and SCDM cosmologies respectively. Since we adopt $N_{\text{SPH}} = 32$, the smallest resolved objects have a gas mass of 4.5×10^{10} and $3.2 \times 10^{10} h^{-1} M_\odot$ in the two cosmologies. An unevolving gas metallicity of 0.3 times the Solar value was assumed, taking into account that gas cooling in objects above the resolution threshold will already have been processed by several previous levels of the merger hierarchy. The SPH simulations use a cooling function which is a series of power-law fits to the results of Raymond, Cox & Smith (1976). If instead the tabulated cooling function of Sutherland & Dopita (1993) is used (this being the function used in the semi-analytic models) then around 10% more cold gas results by $z = 0$ (Kay et al. 2000).

We employed a comoving β -spline gravitational softening equivalent to a Plummer softening length of $35h^{-1} \text{ kpc}$ for $z > 2.5$ in Λ CDM and $25h^{-1} \text{ kpc}$ for $z > 1.5$ in SCDM. At lower redshifts, the softening remained fixed at $10h^{-1} \text{ kpc}$ in physical coordinates, and the minimum SPH spatial resolution was also set to match this value. Approximately 10,000 timesteps were used in each simulation to evolve from $z = 50$ to $z = 0$. With our chosen parameters, the simulations are able to follow the cooling of gas into galactic dark matter halos. The resulting “galaxies” typically have 50-1000 particles.

Dark matter halos were identified at $z = 0, 0.1, 0.2, 0.3, 0.5, 1, 2$ and 3 . Simulation outputs at higher redshifts were available, but so few galaxies have formed beyond $z = 3$ in these small volumes that no statistically meaningful comparison could be made at higher redshifts. Halos were found using the friends-of-friends (FOF) group finding algorithm (Davis et al. 1985) with a linking length of $b = 0.2$ times the mean interparticle separation in SCDM. In Λ CDM, we assume halos form with the overdensity predicted by the model of Eke, Cole & Frenk (1996) and therefore use a linking length which grows from $b = 0.164$ at $z = 0.0$ to $b = 0.200$ at $z = 3$. Consistent definitions of halo overdensities are adopted in the semi-analytic models considered.

“Galaxies” were also found using this algorithm, but with a much smaller linking length of $b = 0.0168$. Galaxies are made of gas particles that have cooled below 12,000 K and represent overdensities of $\gtrsim 100,000$. A complete description of the simulations and the properties of the simulated galaxies is given by Pearce et al. (2000).

2.1.3 Assumptions and Limitations

The key assumption of the SPH technique is that the evolution of gas may be approximated by the evolution of a set of particles. Each particle may be thought of as a packet of gas that “carries” with it the thermodynamical properties of the system.

The smoothing inherent in the SPH technique introduces problems whenever gas properties vary discontinuously (or at least on scales much smaller than the smoothing scale). In the case of shocks, an artificial viscosity term is used to capture the shock and prevent it from being smoothed away by the SPH algorithm. Another example of this kind of problem occurs in a multiphase gas (although see Ritchie & Thomas 2000), in which the sharp boundary between phases is smoothed over, causing the phases to diffuse into one another. This problem can lead to runaway cooling in the centres of dark matter halos, as happened, for example, in one of the simulations of Frenk et al. (1996). The simulations of Pearce et al. (1999) attempt to circumvent this problem by ignoring the contribution of cold ($T < 12,000 \text{ K}$) particles in the computation of the densities of hot ($T > 10^5 \text{ K}$) particles. (For a complete discussion of this approximation see Thacker et al. 1998) An important consequence of this approximation is that galaxies in the simulations match the shape of the observed galaxy luminosity function at the bright end.

A further limitation arises from the fact that the sizes of the galaxies that form in the simulations are determined primarily by the gravitational force softening length rather than by any real physical process. This raises the possibility of enhanced tidal disruption, drag, and merging within dark matter halos. Whilst the softening length is kept fixed in physical coordinates at low redshift, it is fixed in comoving coordinates at high redshift, as described in §2.1.2. Thus for $z > 1.5$ the *physical* softening length in the Λ CDM simulation is larger than in the SCDM simulation and, as a result, non-physical effects due to softening may be expected to be more pronounced at early times in the Λ CDM simulation.

Although a variety of prescriptions have been tried in attempts to model supernovae feedback in SPH simulations, usually by converting cold gas into “star particles” which then inject thermal and kinetic energy into the surrounding gas (e.g. Navarro & White 1993; Steinmetz & Müller 1995; Katz, Weinberg & Hernquist 1996), this process remains poorly understood. In cosmological SPH simulations, gas can only begin to cool efficiently in objects well above the minimum resolved halo mass, around several times $10^{11} h^{-1} M_\odot$ in our case. Thus, resolution effects prevent all the gas from cooling in small halos at high redshift, a process that, in reality, is probably due to feedback from supernovae or other energetic sources. The resolution of our simulation was, in fact, chosen to ensure that the fraction of baryons that cools by the present in the SCDM model is comparable to the observed fraction of cold gas and stars in galaxies

today. This was achieved by carrying out several test simulations with varying resolution until the desired cold gas fraction was obtained (Kay et al. 2000).

2.2 Semi-analytic models of galaxy formation

2.2.1 Techniques

In semi-analytic models, some of the processes involved in galaxy formation (e.g. the growth of dark matter halos by mergers of smaller halos) are followed using analytic solutions and Monte-Carlo techniques. Other, more uncertain processes, such as feedback from supernovae are modelled by means of simple, physically motivated rules. Typically, each such rule contains one or two free parameters which are constrained using observations of galaxies in the local Universe (e.g. Cole et al. 2000).

In semi-analytic models, the dynamics of the gas are strongly coupled to the evolution of dark matter halos and to the processes of star formation and feedback. The starting point for our own modelling is the set of dark matter halos at $z = 0$ drawn from the Press-Schechter mass function. A merging history for each halo is then constructed using the extended Press-Schechter formalism. Beginning with the earliest progenitor halo, our model assumes that gas (initially assumed to have zero metallicity) is shock-heated to the virial temperature of the halo, after which it begins to cool according to a specified cooling function. Any gas that does cool forms a galaxy at the centre of the halo within which stars begin to form at a specified rate, producing both metals and supernovae. Supernovae reheat some of the gas in the galaxy, ejecting it back out into the surrounding halo. (This gas is not allowed to cool again until the halo has merged to form part of a larger halo.) These processes continue until the halo mass has increased by a factor of two or more, either by merging with a larger halo, or by numerous accretions of smaller halos. Any leftover hot gas becomes part of the new halo, and the largest galaxy of the newly formed halo becomes the central galaxy, onto which further gas can cool. Any other galaxies become satellites in the new halo, and may eventually merge with the central galaxy due to energy loss by dynamical friction. The full model includes other processes such as stellar population synthesis and morphological evolution which are not directly relevant to the present work.

As well as this “full” semi-analytic (FSA) model, for the purposes of this work we have constructed a “stripped-down” semi-analytic (SDSA) model which is designed to be directly comparable to the SPH simulations (in a statistical sense). In the SDSA model, we switch off star formation and the associated supernovae feedback and chemical enrichment, since these processes are not included in the SPH calculation. Instead, we assume a fixed metallicity of 0.3 times the Solar value, just as in the simulations. We also mimic the SPH resolution by truncating halo merger trees at N'_{SPH} times the dark matter particle mass in the simulation, and by switching off gas cooling when the hot gas mass is less than N'_{SPH} times the gas particle mass. The parameter N'_{SPH} is set to $2 \times N_{\text{SPH}} = 64$, i.e. twice the number of particles in the SPH smoothing kernel. This value was chosen since it allows the SDSA model to match the position of the peak in the galaxy mass function in the SPH simulations

(as will be shown in §3.2.1, see Fig. 7). The FSA model has no such truncation of merger trees and has effectively unlimited resolution (in practice, we resolve progenitor halos down to masses several hundred times smaller than in the SPH and SDSA models).

To further emulate conditions in the SPH simulations in the SDSA model, we replace the Press-Schechter formula for the mass function of dark matter halos (which is commonly used in semi-analytic models, including our FSA model) with the formula proposed by Sheth, Mo & Tormen (1999) which provides a better match to the results of large N-body simulations (Jenkins et al. 2000). Although this ensures that the abundance of halos at $z = 0$ in the SDSA model is similar to that in the SPH simulations, it does not guarantee that the distribution of progenitor halo masses will also be the same. In fact, as has been shown by Somerville et al. (2000), we find that at high redshifts the merger trees in our SDSA model underpredict the abundance of progenitor halos seen in the SPH simulations. We reconcile the progenitor distributions in the two models by adopting a simple, empirical correction. We scale the value of the extrapolated critical linear threshold for collapse from the spherical collapse model, δ_c , by a redshift-independent factor, f_{δ_c} , such that $\delta_c^{\text{eff}} = f_{\delta_c} \delta_c$. (Thus, in the standard form of the extended Press-Schechter theory, $f_{\delta_c} = 1$.) This approach is similar to that proposed by Tormen (1998). The factor f_{δ_c} is allowed to be a function of the $z = 0$ halo mass. We find that the following simple form for f_{δ_c} provides a reasonable fit to progenitor mass functions in the SPH simulations over the redshift range 0 to 3:

$$f_{\delta_c} = \begin{cases} 1 + 0.09 \left[\log(M_{\text{halo}}/h^{-1}M_{\odot}) - 16.56 \right], & \text{SCDM} \\ 1 + 0.14 \left[\log(M_{\text{halo}}/h^{-1}M_{\odot}) - 15.64 \right], & \Lambda\text{CDM}. \end{cases} \quad (1)$$

This correction to the extended Press-Schechter theory is based purely on an empirical fit to our two simulations. It is designed to minimize differences in the statistical properties of the dark halos in the two models, so that we can focus on differences in their gasdynamical properties. Given the limited statistics provided by our relatively small simulation volumes, this correction should not be regarded as appropriate in a general sense and may not be accurate for larger volumes or for different power spectra to those considered here. In Fig. 1 we show the mass function of progenitor halos at $z = 2$ for parent halos in the mass ranges 10^{12} – $10^{13}h^{-1}M_{\odot}$ and 10^{13} – $10^{14}h^{-1}M_{\odot}$, defined so that $(dN(M_P)/d \ln M_P)d \ln M_P$ is the number of progenitors in the mass range $\ln M_P$ to $\ln M_P + d \ln M_P$ per parent halo. The dashed lines indicate the distribution from our SDSA model with the above correction, whilst the solid lines show the model without the correction. The correction succeeds in ensuring that the mass functions of progenitor halos are statistically similar in the SDSA and SPH models.

2.2.2 Specifics

The semi-analytic model of Cole et al. (2000) was used to simulate galaxy formation in a large sample of dark matter halos spanning a wide range in mass. Specifically, for the SDSA model we simulated halos in 28 mass bins spaced uniformly in the logarithm of halo mass between 10^{11} and $10^{15}h^{-1}M_{\odot}$. For each mass bin, 100 halos were simulated. In the FSA model the mass range was extended down to

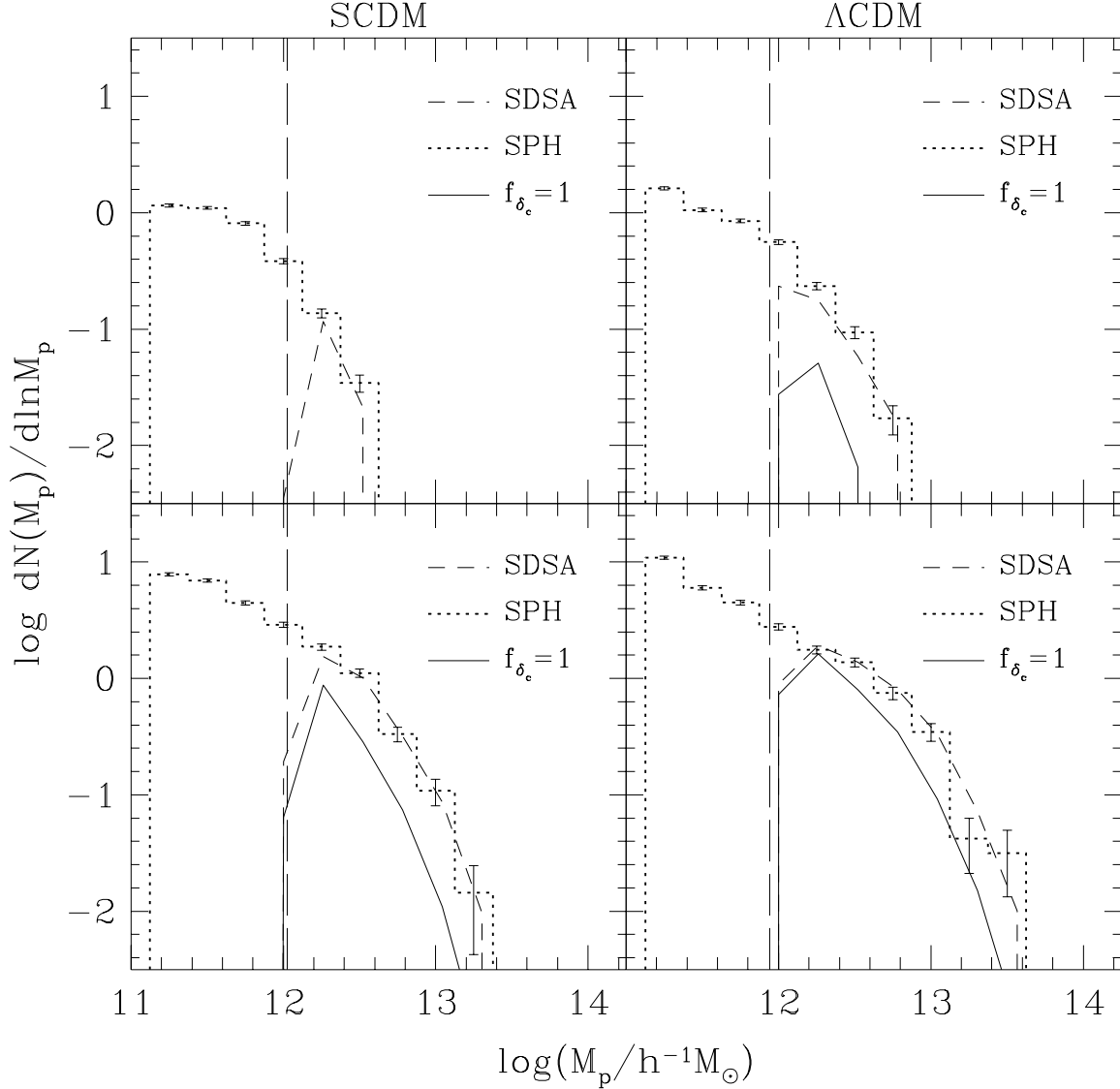


Figure 1. The mass function of dark matter halos at $z = 2$ which are progenitors of present-day halos of mass 10^{12} – $10^{13} h^{-1} M_{\odot}$ (upper panels) and 10^{13} – $10^{14} h^{-1} M_{\odot}$ (lower panels) in the SCDM (left-hand panels) and Λ CDM (right-hand panels) cosmologies. The dotted histograms are the mass functions in the SPH simulations. The thin solid lines show the mass functions obtained from the SDSA models using the standard definition of the extrapolated critical linear overdensity for collapse from the spherical collapse model (i.e. with the parameter $f_{\delta_c} = 1$), whilst the dashed lines show the SDSA model result when f_{δ_c} is chosen to give a good match to the progenitor mass function in the SPH simulations (c.f. eqn. 1). Vertical dashed lines show the resolution limit imposed on the SDSA model merger trees.

$10^{10} h^{-1} M_{\odot}$, and between 4 and 20 halos were simulated in each mass bin (fewer halos were simulated for the most massive bins as these are computationally more expensive). To study the clustering of galaxies in the semi-analytic models, we used the techniques of Benson et al. (2000a,b) and populated halos in the SPH simulations with “semi-analytic” galaxies.

The cosmological parameters required as input into the semi-analytic model ($\Omega_0, \Lambda_0, h, \sigma_8, \Omega_b$) were set to the same values used in the SPH simulations. The remaining parameters of the FSA model were set equal to the values chosen by Cole et al. (2000) (for Λ CDM) and by Benson et al. (2000a) (for SCDM, for which we used the parameters of

their τ CDM model). Parameters were chosen so as to obtain a model which produces a reasonable match to the local B and K-band luminosity functions and other local data (as described by Cole et al. 2000). These parameters can be split into two classes: those that affect the results of the SDSA model and those that do not. The latter, however, are still important for specifying the behaviour of the FSA model. Parameters that do not affect the SDSA model are those which govern star formation, feedback from supernovae and the production of metals by stars. We do not discuss them in any detail here but refer the reader to Cole et al. (2000) for a full description.

The parameters which do affect the results of the SDSA

model (and whose specific values tend to be inspired by the results of simulations) are the following: (i) f_{df} , the dynamical friction coefficient that determines the merger timescale for galaxies orbiting in halos (see eqn. 5); (ii) the dark matter density profile; (iii) the gas density profile; (iv) the progenitor halo mass resolution; and (v) the critical mass for cooling ((iv) and (v) are both specified by N'_{SPH}). Unless otherwise stated, we set $f_{\text{df}} = 1$, $N'_{\text{SPH}} = 64$, and assume (a) that the dark matter density profile has the form proposed by Navarro, Frenk & White (1996,1997, hereafter NFW), namely,

$$\rho(r) \propto \frac{1}{r/r_s(1 + [r/r_s]^2)}, \quad (2)$$

where r_s is a scale-length, and (b) that the gas density has an isothermal profile at large radii, and a constant density core of size r_c , i.e.

$$\rho(r) \propto \frac{1}{r^2 + r_c^2}. \quad (3)$$

The core radius is initially set to some fraction of the NFW scale-length, r_s , of the dark matter halo. Our standard choice for this fraction is 0.33, motivated by the results of hydrodynamical simulations of cluster formation (Navarro, Frenk & White 1995; Eke, Navarro & Frenk 1998). The gas that is able to cool in a halo is the densest gas, which has the lowest entropy. When halos merge to form a new halo this low entropy gas, which would normally settle into the inner parts of the halo, is missing. We take this into account by increasing the core radius of later generations of halos so that the gas density at the virial radius is the same as it would have been if no gas had cooled in progenitors (for a full description see Cole et al. 2000). The model also allows us the option of keeping the core radius fixed, which we explore below. The inclusion of a core in the hot gas profile prevents the formation of extremely bright galaxies in the centres of groups and clusters, which would otherwise lead to a disagreement with the shape of the bright end of the observed galaxy luminosity function. The reasons for choosing this particular profile are therefore identical in spirit to those for preventing runaway cooling in the SPH simulations (see §2.1.3).

2.2.3 Assumptions and Limitations

Semi-analytic models make several assumptions in the treatment of gas in order to obtain simple, analytic solutions to complex hydrodynamical processes. We have already mentioned the important assumptions of spherical symmetry and of the shock-heating of the gas to the virial temperature of its associated halo. The hot gas is then further assumed to settle into a distribution with a universal form. Finally, the amount of gas that is able to cool by time t after the formation of the halo is identified with the gas contained within the radius at which the cooling time equals t . Once it has cooled, this gas is assumed to flow to the centre of the halo, where it is available for star formation, provided that the free-fall time for the gas is also less than t . We shall refer to this as the ‘‘cooling radius’’ prescription.

3 COMPARISON OF THE TWO MODELS

In this section we compare several properties of the galaxy populations that form in our models and consider how this comparison is affected by varying certain assumptions and parameter values.

3.1 Properties of halo gas

We begin by comparing the most basic quantities calculated by each technique, namely the fraction of gas in the hot and cold phases, both globally and as a function of dark matter halo mass. For these purposes, we define a ‘hot halo gas phase’ as gas hotter than 10^5K ; a ‘galaxy phase’ represented by cool, dense gas in the SPH simulation and SDSA, and also including stars in disks and spheroids in the FSA; and an ‘uncollapsed gas phase’ consisting of everything else — i.e. gas outside virialised halos. Note that for the galaxy phase, we consider only galaxies with a mass greater than N'_{SPH} gas particles in the SPH and SDSA models, but include galaxies of all masses in the FSA model.

In the Press-Schechter (or Sheth-Mo-Tormen) theory, all the matter in the universe is deemed to be in halos of some mass, and semi-analytic models assume that gas in halos is shock heated to the halo virial temperature. We can therefore determine the fraction of gas in the uncollapsed gas phase in the FSA model simply by integrating over the analytical mass function (Sheth, Mo & Tormen 1999) from zero mass to the mass corresponding to a virial temperature of 10^5K . According to the spherical top-hat model of halo formation, the mass corresponding to 10^5K is:

$$M_{10^5\text{K}} = 3.5 \times 10^{10} (1+z)^{-3/2} \Omega_0^{-1/2} \left(\frac{200}{\Delta_c(z)} \right)^{1/2} h^{-1} M_\odot, \quad (4)$$

where $\Delta_c(z)$ is the overdensity of a newly formed, virialised dark matter halo at redshift z (e.g. Eke, Cole & Frenk 1996). Since some halos hotter than 10^5K are not resolved in the SDSA model, the integration in this case is carried out from zero mass to $M_{10^5\text{K}}$ or to N'_{SPH} dark matter particle masses, whichever is largest. This estimate does not correspond exactly to the situation in the SPH simulation in which the largest halos are surrounded by gas at temperatures above 10^5K which extends beyond the virial radius. Because of this, the SDSA model calculation will effectively overestimate the amount of uncollapsed gas relative to the SPH simulation. On the other hand, gas in the SPH simulation tends to be slightly more extended than assumed in the semi-analytic model (i.e. the simulated clusters tend to have a baryonic content slightly smaller than the universal baryon fraction within a radius enclosing an overdensity of 200 — see e.g. Frenk et al. 1999). These two effects counteract each other to some degree.

The amount of gas in the hot and galaxy phases depends upon the rate at which gas cools. Therefore this comparison tests model assumptions relating to the process of gas cooling, such as spherical symmetry and the cooling radius prescription in the semi-analytic models or the effects of smoothing in SPH. This test will therefore be sensitive to the choice of gas density profile in the semi-analytic models and to N_{SPH} in the simulations. Since this comparison is concerned only with the total amount of gas in different

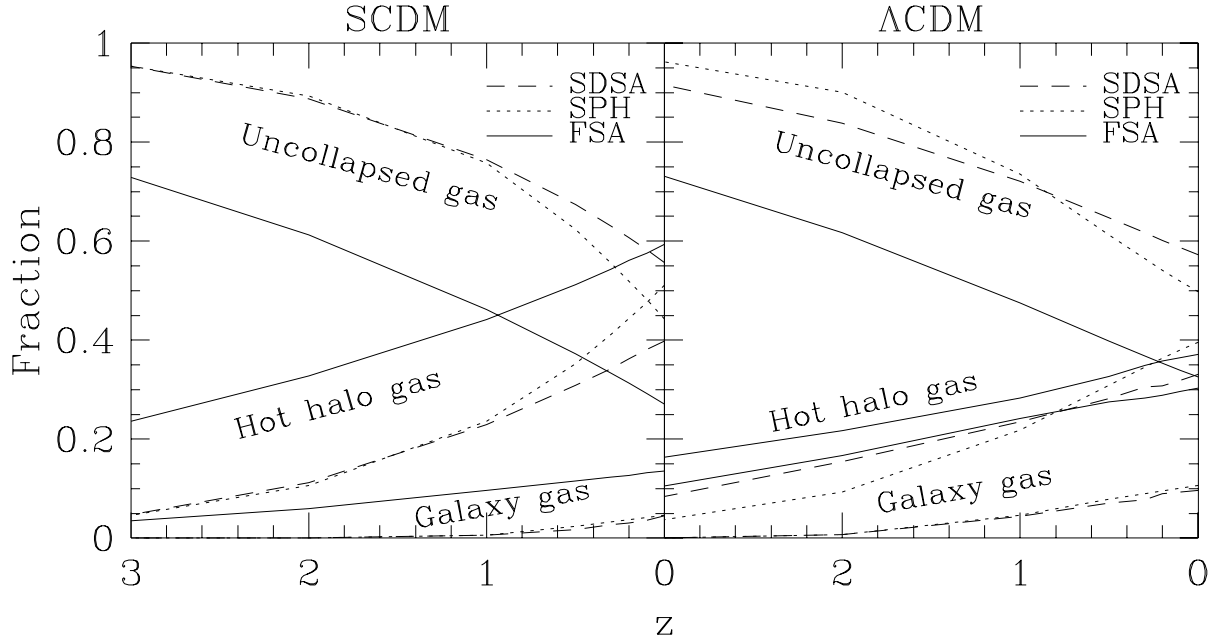


Figure 2. The global fraction of gas in each of three phases: hot halo gas, uncollapsed gas and galaxy gas. Dotted lines correspond to the SPH simulation, dashed lines to the SDSA model, and solid lines to the FSA model.

phases, it is insensitive to the way in which the gas is apportioned into galaxies within a single halo, at least in the SPH and SDSA models. In the FSA model, some dependence on galaxy merger rates may exist, since merging can affect the star formation rate in a galaxy and thus alter the amount of gas reheated by feedback, as well as the rate of chemical evolution, which in turn alters the cooling rates in subsequent generations of halos.

3.1.1 Global gas fractions

Figure 2 shows the fraction of gas in each of the three phases: hot halo, galaxy and uncollapsed, as a function of redshift. In both cosmologies, the uncollapsed gas fraction in the SDSA model is quite close to, although somewhat larger (by $\lesssim 0.1$), than in the SPH simulation at low redshifts. At $z = 0$, the fractional difference is $\lesssim 30\%$. Given the caveats mentioned above, this level of agreement is pleasing. In the FSA model, the fraction of gas in the uncollapsed phase is significantly lower than in the SPH simulation and the SDSA models. The only differences between the FSA and SDSA models in this calculation is the numerical resolution and the use of the Press-Schechter mass function in the FSA model and the Sheth-Mo-Tormen in the SDSA model. It turns out that these differences contribute about equally to the discrepancy in the fraction of uncollapsed gas in the two cases at $z = 0$. (The Press-Schechter mass function contains more low temperature halos than the Sheth-Mo-Tormen mass function.) At higher redshift, resolution effects are the dominant factor. The gas belonging to sub-resolution halos is classed as uncollapsed gas in the SDSA and SPH cases, but is accounted for as hot halo or galaxy gas in the FSA case.

In the galaxy phase, which is the most interesting from the perspective of galaxy formation, the SDSA and SPH models again agree extremely well at all redshifts

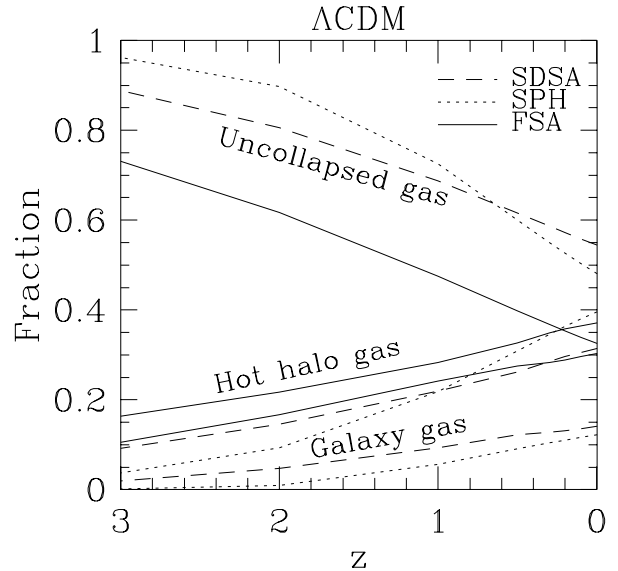


Figure 3. The global fraction of gas in each of three phases: hot halo gas, uncollapsed gas and galaxy gas. Results are shown for the Λ CDM cosmology with $N'_{\text{SPH}} = 32$. Dotted lines correspond to the SPH simulation, dashed lines to the SDSA model, and solid lines to the FSA model.

in both cosmologies. The fractional difference, defined as $|M_{\text{SDSA}} - M_{\text{SPH}}|/M_{\text{SPH}}$ where M_{SDSA} and M_{SPH} are the masses of galaxy gas in the SDSA and SPH models respectively, is close to 50% at $z = 2$ in the SCDM cosmology, but is much smaller in Λ CDM. Half of the $z = 0$ mass of galaxy gas has cooled by $z \approx 0.5$ and $z \approx 1.0$ in SCDM and Λ CDM respectively. Below these redshifts, the fractional difference between the SDSA and SPH models is everywhere less than

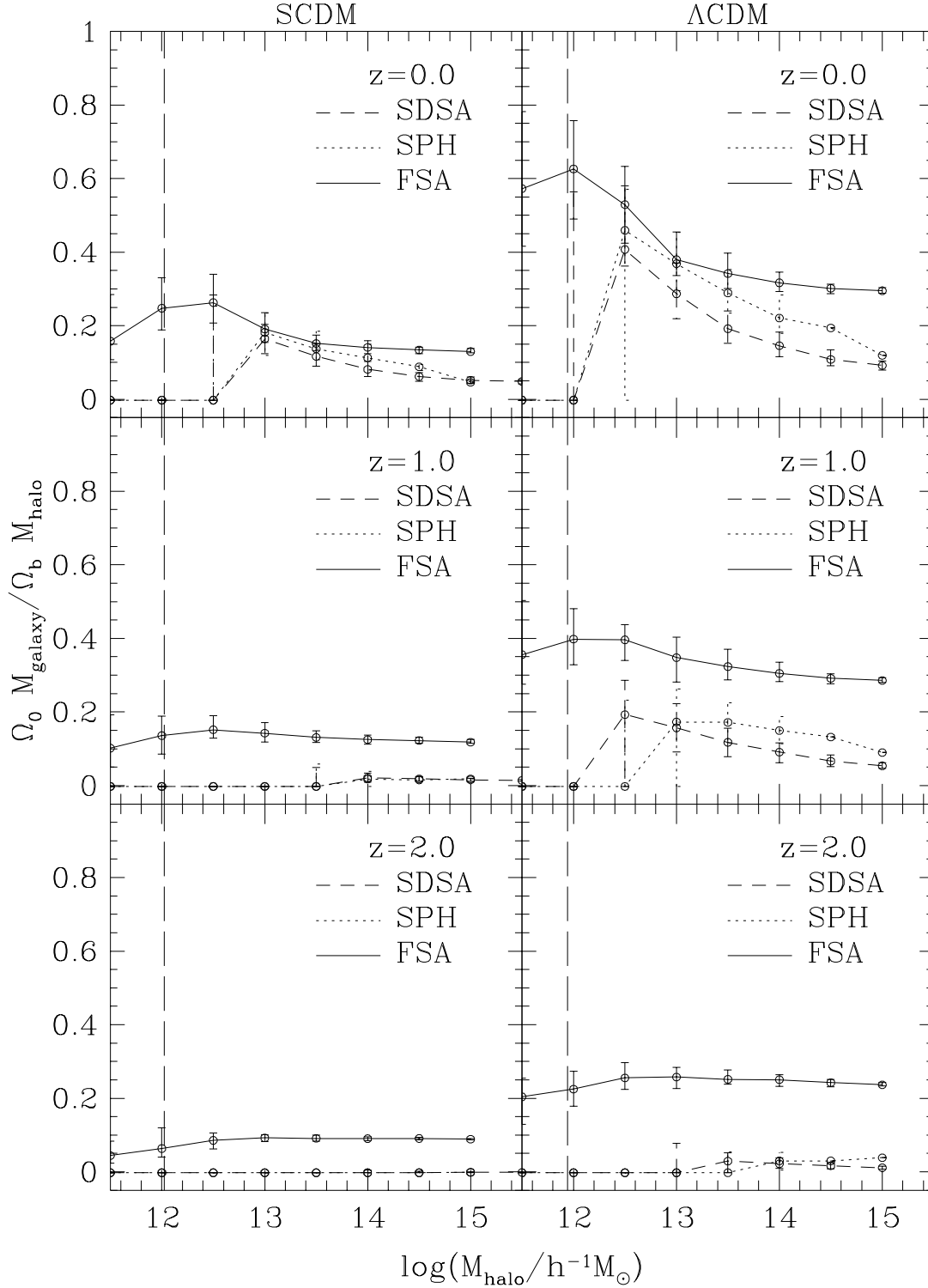


Figure 4. The mass of gas relative to the total halo mass (i.e. dark matter plus gas) at $z = 0$ in progenitor galaxies, as a function of present-day halo mass. (At $z = 0$ we include all galaxies in the halo, whilst at higher redshifts we include all galaxies in progenitors of this halo.) The ordinate shows this fraction divided by the universal baryon fraction. Only progenitor galaxies more massive than N'_{SPH} gas particles are considered. Results are shown at $z = 0, 1$ and 2 for SCDM (left-hand panels) and Λ CDM (right-hand panels). The solid lines show the median of the distribution in the FSA model, with errorbars indicating the 10 and 90 percentiles. The dotted lines show the corresponding fraction for galaxies in the SPH simulation, and the dashed lines for galaxies in the SDSA model. The long-dashed, vertical lines indicate the mass of those halos which, on average, contain a total gas mass (including the hot and cold components) equal to 64 times the SPH gas particle mass (assuming that the gas mass is Ω_b/Ω_0 times the total halo mass).

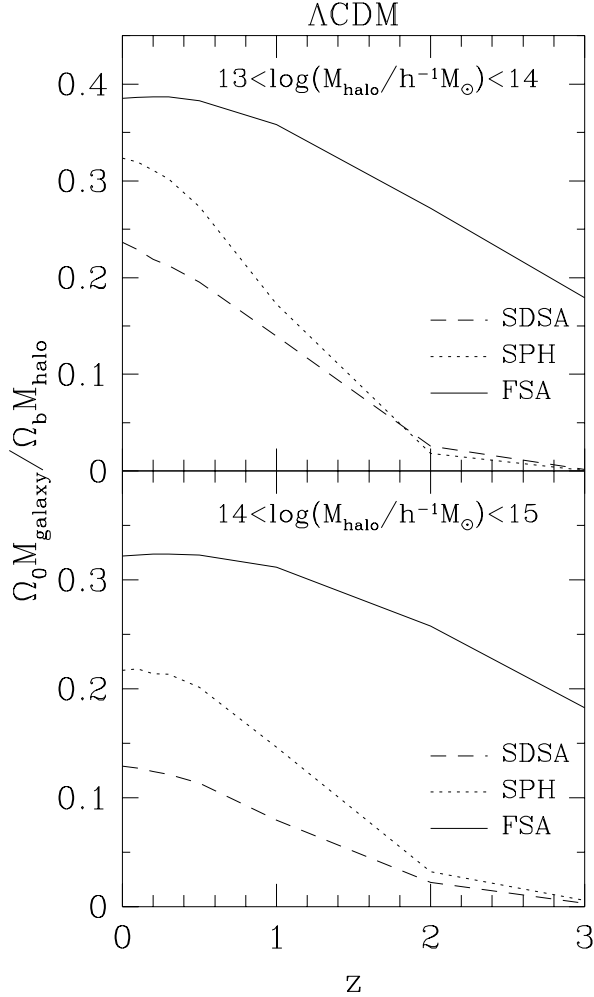


Figure 5. The mean mass of gas in the galaxy phase relative to the total mass (i.e. dark matter plus gas) of the $z = 0$ halo, scaled by the universal baryon fraction, as a function of redshift in progenitors of present-day halos of mass 10^{13} – $10^{14} h^{-1} M_{\odot}$ (upper panel) and 10^{14} – $10^{15} h^{-1} M_{\odot}$ (lower panel). Results are shown for the Λ CDM cosmology. Dashed lines show the SDSA models, dotted lines the SPH models and solid lines the FSA models.

25%. The agreement between the hot halo gas in the SDSA and SPH models is also very good. For Λ CDM, at $z = 0$, the two models differ by only 20%. This is a non-trivial result. One of the most uncertain assumptions of the semi-analytic technique is that gas is shock-heated to the virial temperature of the parent halo. It is therefore reassuring that the amount of hot halo gas turns out to be similar to that seen in the SPH simulations.

The FSA model predicts significantly more galaxy gas than the SPH and SDSA models. Since the merger trees in this model have effectively no mass resolution limit, gas cools very efficiently at high redshifts in small halos. However, feedback reheats a significant fraction of this gas, reducing the galaxy phase fraction. In SCDM, stronger feedback is required to match the observed galaxy luminosity function than in Λ CDM, and this is reflected in a smaller galaxy gas fraction.

Since it is N'_{SPH} that determines which halos are re-

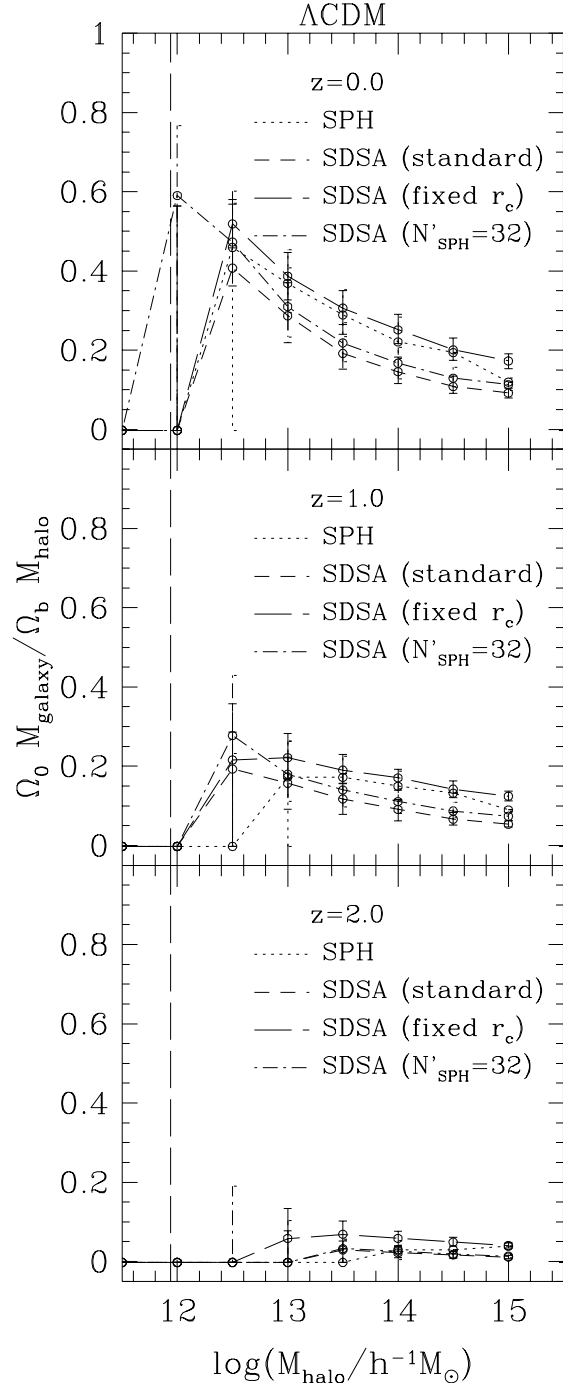


Figure 6. The mass of galaxy gas relative to the total halo mass (i.e. dark matter plus gas) at $z = 0$ in progenitor galaxies, as a function of present-day halo mass in the Λ CDM cosmology. (At $z = 0$ we include all galaxies in the halo, whilst at higher redshifts we include all galaxies in progenitors of this halo.) The ordinate shows this fraction divided by the universal baryon fraction. The dotted line shows the median, and the errorbars the 10 and 90 percentiles of the distribution in the SPH simulation. The remaining lines show predictions calculated from the SDSA model for: standard parameters (dashed line); a hot gas core radius which is fixed at 0.33 times the NFW scale length (long-dashed line); and a critical mass for cooling equal to 32 times the SPH gas particle mass (dot-dashed line). The long dashed, vertical line indicates the mass at which halos contain a total mass in gas (i.e. hot halo and galaxy gas) equal to 64 times the SPH gas particle mass (assuming that the gas mass is Ω_b/Ω_0 times the total halo mass). Results are shown at $z = 0, 1$ and 2 as indicated in the panels.

solved in the SDSA model, this parameter affects the gas fractions in all three phases. For example, reducing N'_{SPH} from 64 to 32 worsens the agreement between the galaxy phase fractions in the SDSA and SPH models in the Λ CDM cosmology as shown in Fig. 3, although the two models are still reasonably close, differing only by approximately 15% at $z = 0$. The differences produced by this entirely plausible change in N'_{SPH} are indicative of the degree of uncertainty inherent in these comparisons.

3.1.2 Galaxy gas fractions in halos

Figure 4 shows the mass of “galaxy-phase” gas, expressed as a fraction of the total (i.e. dark matter plus gas) halo mass and scaled by the universal baryon fraction. At $z > 0$ the quantity shown is the fraction of gas which exists in progenitors of the $z = 0$ halos in each mass bin. This is a bulk quantity for each halo and is independent of the way in which gas is divided among the galaxies that reside in each halo. The SDSA model predicts somewhat less galaxy gas than the SPH simulation, particularly in the Λ CDM cosmology. The difference is typically $\sim 50\%$, except at low masses where the agreement is better. (We do not plot error bars for the largest mass bins in the SPH simulations because they contain only one or two halos.) We note that this is significantly more than the 10% change in cooled gas mass found by Kay et al. (2000) when the Sutherland & Dopita (1993) cooling function was used in SPH simulations (which, in any case, increased the amount of gas that cooled). At higher redshifts, the two model curves become closer, indicating different mean rates of gas cooling. At the smallest masses plotted, the SPH and SDSA curves turn over near the critical cooling mass (marked on the plot by the vertical long dashed line) because of resolution effects, while the FSA model turns over because of the effects of feedback which begin to become efficient at reheating cold galaxy gas in halos below $\sim 10^{12} h^{-1} M_{\odot}$.

As noted in §3.1.1, the FSA model cools much more gas into the galaxy phase than the SPH and SDSA models. Much of this gas cools at high redshift in low mass progenitor halos (which are unresolved in the SDSA and SPH models) as may be seen from the lower panels of Fig. 4.

Differences in the cooling rates in the Λ CDM cosmology can be seen more clearly in Fig. 5, where we plot the mean fraction of cold gas in progenitor galaxies for two bins of present-day halo mass: 10^{13} – $10^{14} h^{-1} M_{\odot}$ (upper panel) and 10^{14} – $10^{15} h^{-1} M_{\odot}$ (lower panel). At high redshifts, the SPH cooling rate is very similar to the cooling rate in the SDSA model, but it becomes faster at lower redshifts. Similar trends are seen in the SCDM cosmology, although the differences are smaller, leading to very similar present-day gas fractions in the two models. In Λ CDM, the SPH model ends up with 30–70% more cool gas. In both cosmologies, the net cooling rate in the FSA model is slower than in the SPH model (particularly in the lower range of halo mass), but comparable to that in the SDSA model. Whilst the FSA model resolves more progenitors, which speeds cooling, feedback reduces the effective cooling rate. However, since the FSA model contains progenitor halos at much higher redshifts than the other models (due to its greater resolution), more gas has already cooled in the FSA model by $z = 2$ than in either the SPH or SDSA models.

Since the amount of gas that can cool depends upon the density profile assumed for the hot halo and on the critical cooling mass, it is interesting to see how sensitive the agreement between the SDSA model and the SPH simulation is to variations in these parameters. We show the result of this test in Fig. 6 for the Λ CDM cosmology. (The trends are similar for SCDM.) Halving the critical mass required for gas cooling (i.e. reducing N'_{SPH} from 64 to 32) in the SDSA model has a small effect, marginally improving the agreement with the SPH simulation. (Note that for $N'_{\text{SPH}} = 32$, we plot results only for objects more massive than 64 gas particles in order to compare directly to the other curves.) The critical cooling mass is not, of course, a precise number, and this comparison suggests that we may have been too conservative in setting it equal to $2 \times N_{\text{SPH}}$. In any case, it appears that the agreement between the galaxy gas mass as a function of halo mass in the SDSA and SPH models is better than one might have expected.

Keeping the gas core radius fixed at $0.33r_s$ in all halos, rather than letting it grow as in our standard model, allows significantly more gas to cool in the SDSA model. This brings this model into excellent agreement with the SPH model at $z = 0$, as may be seen in Fig. 6, but at the expense of a slightly larger cooled gas mass at higher redshifts. Adopting a smaller core radius (e.g. $r_c = 0.15r_s$) makes very little difference. Finally, we note that assuming a gas profile which traces that of the dark matter leads to $\sim 50\%$ more cooling in the highest mass halos (note this model is not shown in Fig. 6).

3.2 Properties of galaxies

We now consider properties of the models that are sensitive to the way in which gas is apportioned amongst individual galaxies, rather than just the total amount of gas in a halo. In the SPH simulation, the number of galaxies that form in a given halo and their masses are determined by resolution effects, the gas cooling rate and the galaxy merger rate. In the semi-analytic models, the choice of density profile for the hot corona determines the cooling rate of the gas. We also expect the masses and numbers of galaxies to be affected by the choice of f_{df} , which controls the rate at which galaxies merge within a halo and, in the case of SDSA model, the choice of N'_{SPH} , which determines the minimum halo mass in which galaxies can form.

3.2.1 Galaxy mass function

Figure 7 shows the differential galaxy mass functions in the models at $z = 0, 1$ and 2. (Recall that, by definition, M_{galaxy} consists only of cold gas in the SPH and SDSA cases, but can also include stars in a disk and spheroid in the FSA case.) The agreement between the SPH and semi-analytic models is somewhat different in the two cosmologies. In the SCDM case, there is quite good agreement for large galaxy masses, but the SPH simulation produced about twice as many galaxies with mass of a few times $10^{11} M_{\odot}$ than the SDSA model. In the Λ CDM case, the SPH simulation produced about 3–4 times as many galaxies as the SDSA model over most of the mass range above the critical cooling mass. If viewed as a difference in mass at fixed abundance, the

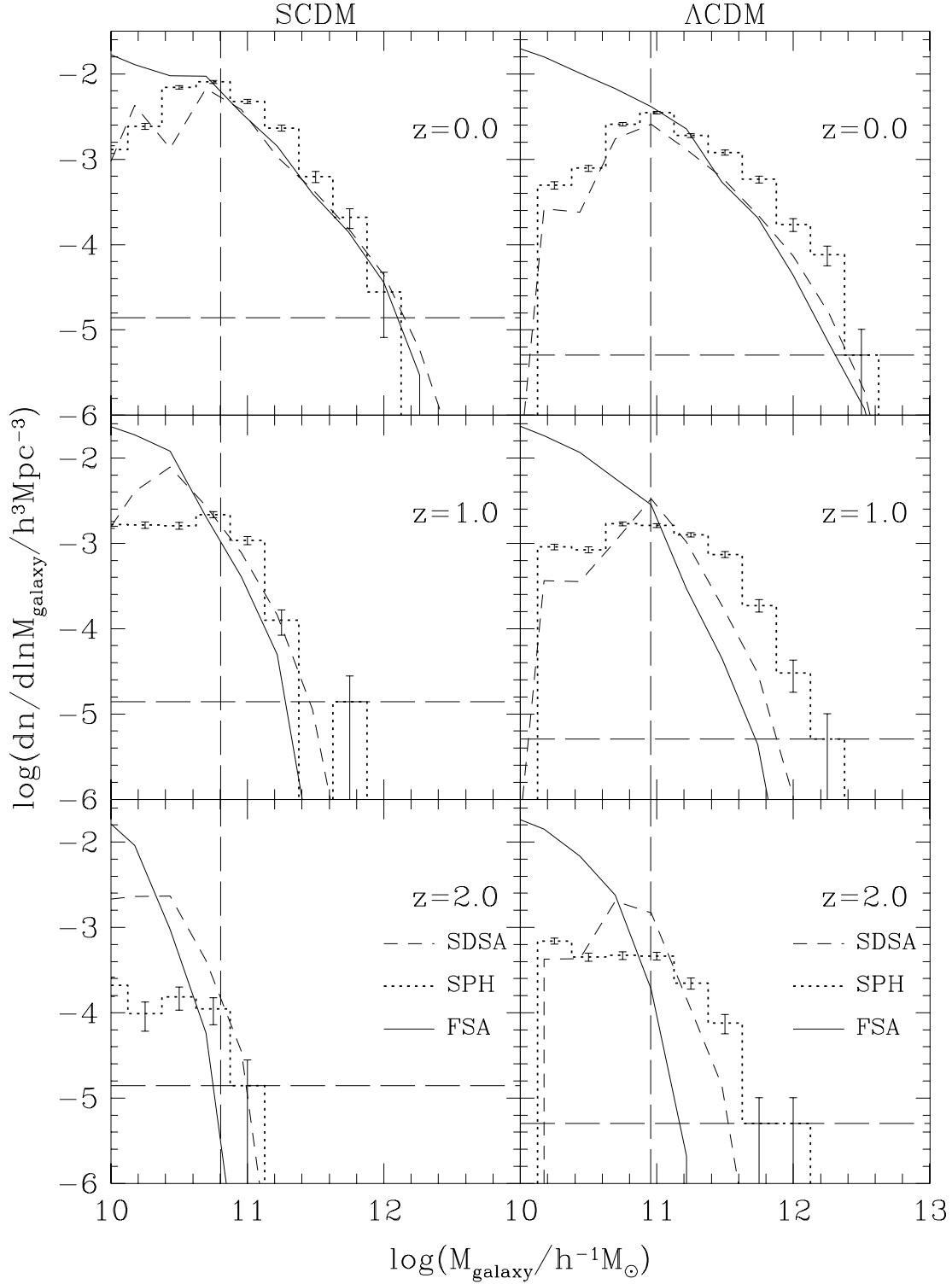


Figure 7. The differential galaxy mass function in the SCDM (left-hand panels) and Λ CDM (right-hand panels) cosmologies at various epochs. The solid line corresponds to the FSA model, the dotted histogram to the SPH simulation and the dashed line to the SDSA model. The vertical dashed line indicates the critical mass for cooling in the SPH simulations (which is 64 times the gas particle mass), whilst the horizontal dashed line indicates the abundance corresponding to one object in the entire SPH simulation volume. Results are shown at $z = 0, 1$ and 2 as indicated in each panel.

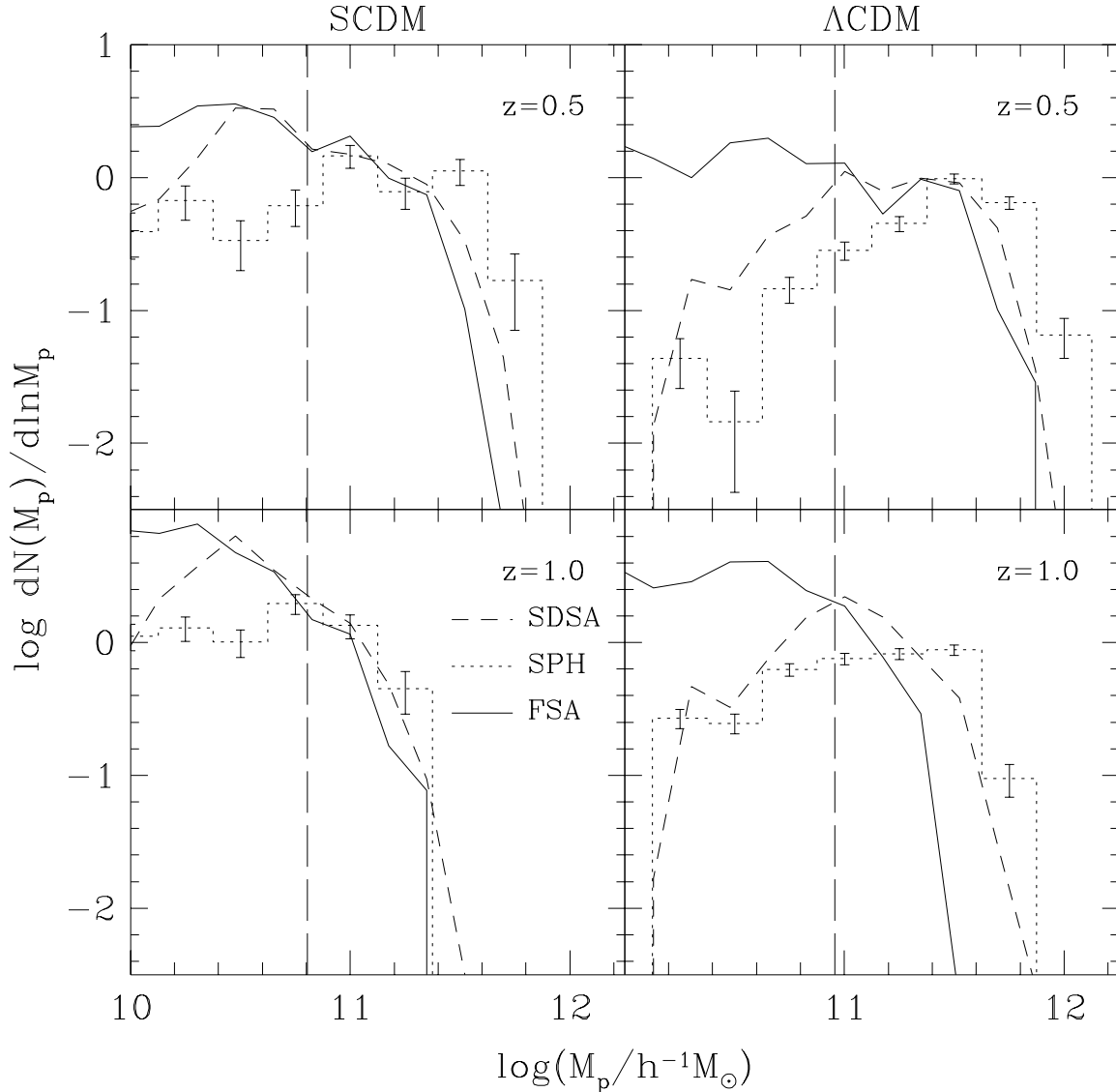


Figure 9. The mass function of galaxies which are progenitors of present-day galaxies with (cold gas plus stellar) masses $10^{11.5}$ – $10^{12} h^{-1} M_{\odot}$. Results are shown at $z = 0.5$ and 1 for SCDM (left-hand panels) and Λ CDM (right-hand panels). The solid line corresponds to the FSA model, the dotted histogram to the SPH simulation and the dashed line to the SDSA model. The vertical dashed line indicates the mass corresponding to 64 SPH gas particles.

discrepancy can be as large as a factor of almost 2. For a fixed mass-to-light ratio, this would lead to the bright end of the luminosity function being approximately 0.75 magnitudes brighter in the SPH simulation than in the SDSA model. The differences between SDSA and SPH models are similar at higher redshifts, whilst the FSA mass function evolves more rapidly. We discuss the possible reasons for these discrepancies shortly.

First, we note the interesting behaviour at the low mass end of the mass function. Below the critical cooling mass, 9.0×10^{10} and $6.4 \times 10^{10} h^{-1} M_{\odot}$ in Λ CDM and SCDM respectively, the abundance of galaxies in the SDSA and SPH models drops very sharply, due to the effects of resolution. These prevent the formation of small halos and also inhibit the cooling of gas in marginally resolved halos. In the FSA

model, on the other hand, the number of galaxies continues to rise towards small masses. Although feedback becomes gradually more efficient towards lower masses, this still allows many low mass galaxies to form. In both the SDSA and SPH models some galaxies do form with mass below the cooling limit. In the former case this can occur because cooling is prevented only in halos with a total hot gas mass lower than the limit. It is still possible for cooling in a more massive halo to create a galaxy below the mass threshold simply because there has not been enough time for the total hot gas mass of the halo to cool. The SPH simulations also contain galaxies below the mass limit because the cutoff is not sharp, but marks the point at which cooling becomes efficient. These objects represent young galaxies in the process of formation and, except at early times, they make up a

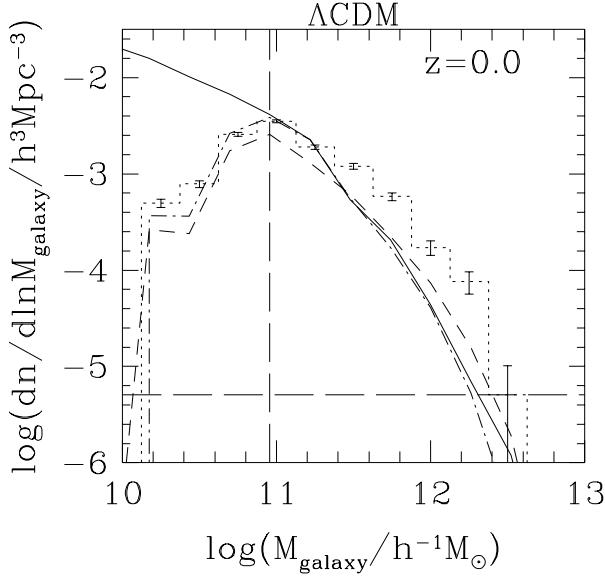


Figure 8. The differential galaxy mass function at $z = 0$ in the Λ CDM cosmology. The solid line corresponds to the FSA model, the dotted histogram to the SPH simulation and the dashed line to the SDSA model. Dot-dashed lines show the results for the SDSA model using the standard Press-Schechter dark matter halo mass function and the standard extended Press-Schechter formalism (i.e. with $f_{\delta_c} = 1$) for generating merger trees. The vertical dashed line indicates the critical mass for cooling in the SPH simulations (which is 64 times the gas particle mass), whilst the horizontal dashed line indicates the abundance corresponding to one object in the entire SPH simulation volume.

small fraction of the total number of galaxies. In addition, in the SPH model there is a small contribution at low masses from galaxies that are being tidally disrupted in clusters.

In Fig. 8 we show the effect on the SDSA galaxy mass function (in the Λ CDM cosmology) of using the standard Press-Schechter halo mass function and $f_{\delta_c} = 1$, rather than the Sheth-Mo-Tormen halo mass function and f_{δ_c} as given by eqn. (1). Using the latter, more accurate, mass function produces somewhat more massive galaxies. The choice of f_{δ_c} alters the mass function of progenitors of the more massive galaxies, but has little effect elsewhere.

Some insight into the origin of the differences between the galaxy mass functions in the SPH and SDSA models may be obtained by considering the mass function of galaxy progenitors. For present-day galaxies with masses in the range $10^{11.5} - 10^{12} h^{-1} M_{\odot}$, Fig. 9 shows progenitor mass functions at $z = 0.5$ and $z = 1$. These are normalized to the present day abundance of galaxies (i.e. $(dN(M_P)/d \ln M_P) d \ln M_P$ is the number of progenitors in the mass range $\ln M_P$ to $\ln M_P + d \ln M_P$ per parent galaxy) so that the differences in the $z = 0$ mass functions seen in Fig. 7 do not propagate through to this comparison. It is immediately obvious from this figure that the SDSA galaxies have fewer high-mass progenitors than the galaxies in the SPH simulation, particularly in the Λ CDM cosmology.

The discrepancy between the SPH and semi-analytic galaxy mass functions seen in Figs. 7 and 9 could be due either to differences in the galaxy merger rates or in the gas

cooling rates in the two models. We first consider the possibility that the SPH and SDSA galaxy merger rates may be different, leading to different numbers of galaxies forming in each halo. As we discussed in §2.1.3, merging in the SPH simulations may be artificially enhanced by non-physical effects introduced, for example, by the use of softened forces. The strength of these effects will depend in a non-trivial way on the formation epoch of each galaxy. Whilst we cannot attempt to mimic the details of such effects in the semi-analytic model, we can explore the consequences of a global change in the merger timescale. In the semi-analytic model, when a galaxy falls into a larger halo, it is assumed to sink to the centre in a time proportional to the dynamical friction timescale for an object orbiting in an isothermal halo. This may be written as (Lacey & Cole 1993):

$$\tau_{\text{mrg}} = f_{\text{df}} \theta_{\text{orb}} \tau_{\text{dyn}} \frac{0.3722}{\ln(\Lambda_{\text{Coulomb}})} \frac{M_{\text{H}}}{M_{\text{sat}}}, \quad (5)$$

where f_{df} is a dimensionless parameter; M_{H} is the mass of the halo in which the satellite orbits; M_{sat} is the mass of the satellite galaxy including the mass of the dark matter halo in which it formed (not including the mass of the satellite's dark matter halo leads to an overestimate of the dynamical friction timescale as shown by Navarro, Frenk & White 1995); τ_{dyn} is the dynamical time of the large halo and the Coulomb logarithm is $\ln(\Lambda_{\text{Coulomb}}) = \ln(M_{\text{H}}/M_{\text{sat}})$. The variable θ_{orb} contains the dependence of the merger timescale on the orbital parameters of the galaxy and is chosen from the distribution found in N-body simulations by Tormen (1997), as described by Cole et al. (2000).

Cole et al. (2000) point out that the formula in eqn. (5) has been derived on the basis of a number of assumptions, for example that the galaxy may be treated as a point mass. Thus, whilst they recommend a default value of $f_{\text{df}} = 1$, they also allow themselves the freedom to choose a different value if required to produce a realistic model. Recently, Colpi, Mayer & Governato (1999) have examined the validity of eqn. 5 in detail using both analytic and numerical techniques. On the basis of their investigations, they suggest small modifications to the formula, in particular a slightly different dependence of θ_{orb} on the orbital eccentricity. They also find that the effects of tidal stripping produce $f_{\text{df}} \approx 2.7$ (for a specific model of the satellite's dark matter halo). Both of these changes act to increase τ_{mrg} , and so reduce the merger rate. Since the SDSA model already contains too few high mass galaxies compared to the SPH simulations, a slower merger rate would merely increase the discrepancy.

At the resolution of our SPH simulations, an infalling satellite galaxy will lose nearly all of its original dark matter halo shortly after entering the larger halo. On the other hand, in the SPH simulations, merging with the central object is driven not only by dynamical friction, but also by drag due to viscous effects as the satellite moves through the hot halo of the cluster (Frenk et al. 1996; Tittley, Couchman & Pearce 1999). These processes may drive the effective f_{df} to a value less than unity.

The smaller the value of f_{df} , the faster a galaxy will sink to the centre of its host halo. In Fig. 10 we show the effect of reducing the merging rate from the default value, $f_{\text{df}} = 1$, to $f_{\text{df}} = 0.4$ on the SDSA galaxy mass function in the Λ CDM model. This change improves the match between the SDSA and SPH models at $z = 0$, but only slightly, and

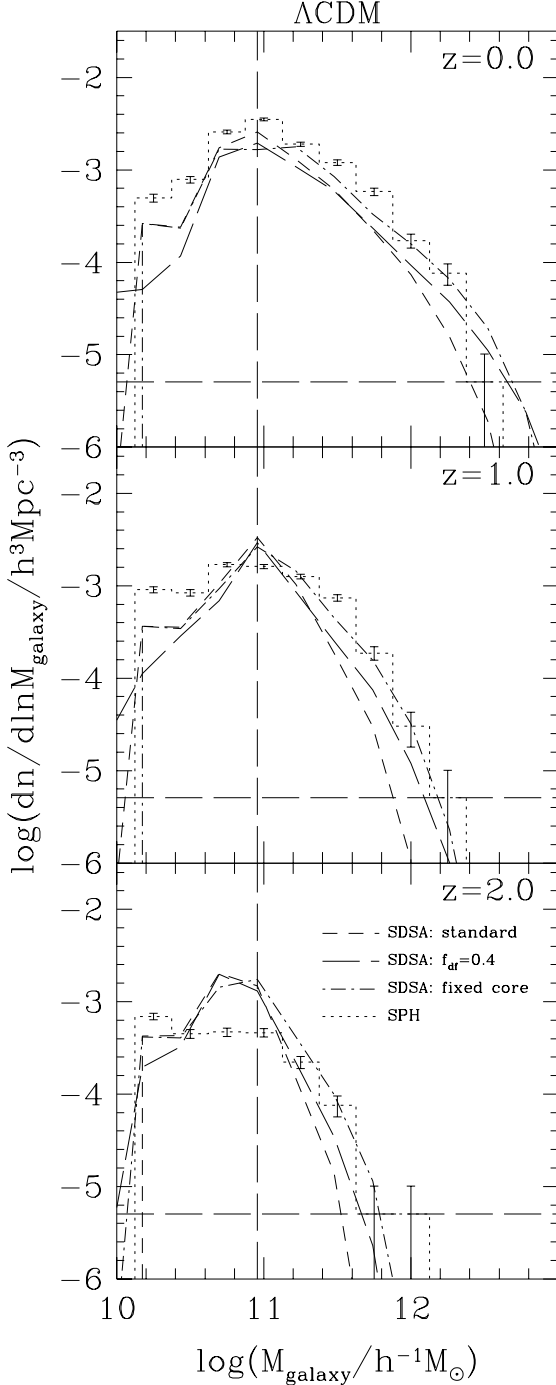


Figure 10. The differential galaxy mass function at selected redshifts in the Λ CDM cosmology predicted by the SDSA model when (i) using a faster merging rate (long-dashed line) and (ii) keeping the core radius of the hot gas density profile fixed (dot-dashed line). For reference, the short-dashed line shows the standard SDSA model. Dotted histograms show the SPH simulation results. The vertical dashed lines indicate the critical mass for cooling in the SPH simulations (which is 64 times the gas particle mass), whilst the horizontal dashed line indicates the abundance corresponding to one object in the entire SPH simulation volume. Results are shown at $z = 0, 1$ and 2 , as indicated in each panel.

mostly at high masses. Below $10^{12}h^{-1}M_{\odot}$, the two models still differ significantly. At higher redshift the improvement is slightly better, but the SDSA model still contains fewer high-mass objects than the SPH simulation. Thus, a change in the global merger timescale does not help to reconcile the two models. This is perhaps not too surprising since this simple alteration cannot mimic any redshift dependence of the merger timescales in the SPH simulation. Decreasing f_{df} further produces more high mass galaxies, at the expense of depleting the number of lower mass galaxies, thereby worsening the agreement between the SDSA and SPH galaxy mass functions at the low mass end.

A second possible explanation for the discrepancy between the galaxy mass functions is that the relative cooling rates in the SPH and SDSA models are different. We investigate the effects of changing the rate at which gas cools in the SDSA model, by keeping the core radius of the hot gas density profile equal to a fixed fraction of the NFW scale radius in the halo. This has the effect of allowing gas to cool more rapidly in any given halo. The galaxy mass function of the SDSA model for this case is shown by the dot-dashed line in Fig. 10. The agreement with the SPH simulation is now much improved.

In the next section we will explore how changing merger and cooling rates affects the number of galaxies found in halos of a given mass and thus identify the underlying cause of the differences between the mass functions in the SDSA and SPH models.

3.2.2 Number of galaxies per halo

The redshift evolution of the mean number of progenitor galaxies per halo in the Λ CDM cosmology is shown in Fig. 11, for two ranges of present-day halo masses: $10^{13}\text{--}10^{14}h^{-1}M_{\odot}$ (upper panel) and $10^{14}\text{--}10^{15}h^{-1}M_{\odot}$ (lower panel). (Qualitatively similar results are obtained for the SCDM cosmology.) In the SPH simulation there are 165 halos in the lower mass range and 12 in the higher mass range. Since the galaxy abundance is a steep function of galaxy mass (c.f. Fig. 7) the number of galaxies per halo above some particular mass cut is always dominated by galaxies close to the cutoff. As a result, the number of galaxies per halo more massive than 64 SPH particles may be affected by differences in the way in which the resolution limit works in SPH and SDSA models. Therefore, we plot results for galaxies more massive than 64 SPH gas particles (thin lines), but also for those more massive than 128 SPH gas particles (heavy lines) which are much less affected by resolution effects.

The shape of the abundance curves in Fig. 11 is determined by the relative rates of galaxy formation and merging and has the same basic form in the SDSA and SPH models. The number of galaxies more massive than 64 SPH gas particles predicted by the SDSA model in halos of mass $10^{13}\text{--}10^{14}h^{-1}M_{\odot}$ at the present day agrees well with that found in the SPH simulation. The level of agreement, however, is less impressive at higher redshift and for higher mass halos. For the 128 particle selection the SDSA model contains *fewer* galaxies per halo than the SPH model in both ranges of halo mass and at all redshifts.

In the preceding subsection, we saw that increasing the merger rate in the Λ CDM SDSA model leads to slightly better agreement between its galaxy mass function and that

of the SPH simulation. A faster merger rate, however, depletes the number of galaxies by combining them into larger galaxies. In Fig. 12, we show the effect of reducing f_{df} from 1 to 0.4 on the evolution of the progenitor population in the SDSA model. For galaxies more massive than 64 SPH gas particles, the rate at which N_{gal} increases at high redshift is now slower than before and results in a lower value of N_{gal} at the present day. The net effect is to bring the SDSA curve closer to the SPH results for the 10^{14} – $10^{15}h^{-1}M_{\odot}$ halo sample, but to increase the discrepancy for the 10^{13} – $10^{14}h^{-1}M_{\odot}$ halos. For galaxies more massive than 128 SPH gas particles, the already low galaxy numbers are depleted even further, exacerbating the discrepancy with the SPH results. We conclude that the discrepancies in the mass functions in the Λ CDM SDSA and SPH models are not due to differences in the galaxy merger rates in the two models.

The effects of altering the cooling rate in the SDSA model are also illustrated in Fig. 12 (dot-dashed lines). As before, we have varied the cooling rate simply by keeping the core radius of the hot gas density profile fixed. For galaxies more massive than 64 SPH gas particles, the SDSA model now overpredicts the mean number of galaxies per halo at all redshifts, particularly in the most massive halos. The increase is driven by galaxies near the 64 particle cutoff whose mass increases due to the additional cooling of gas. (A similar behaviour occurs if the cooling rate is enhanced by reducing the threshold for cooling from $N'_{SPH} = 64$ to 32, rather than by changing the density profile of the gas.)

A cleaner test can be made by looking at galaxies more massive than 128 SPH gas particles. In this regime, the SDSA model with enhanced cooling is in excellent agreement with the SPH simulation. As we saw earlier, such a modification of the SDSA model also produces a galaxy mass function (Fig. 10) and a distribution of cold gas in halos of different mass (Fig. 6) that are very similar to those in the SPH simulation. We conclude therefore that the main reason for the differences we have found between the SDSA model and the SPH simulation is that gas cools more efficiently in massive halos in the SPH simulation. This difference, and the corresponding differences in the mass function, are larger in Λ CDM than in SCDM, presumably because of the larger time interval during which gas can cool in Λ CDM. Increasing the cooling rate in the SDSA model slightly spoils the excellent agreement with the SPH simulation on the global phase fractions (Fig. 2). The effect, however, is small (a maximum difference of 50% as opposed to the original 25%) and of the same order as the effect of assuming a different resolution limit for the SDSA model (Fig. 3).

3.3 Spatial distribution of galaxies

As a final comparison, we consider the clustering of galaxies, as measured by the two-point correlation function. This is plotted in Fig. 13 for galaxies more massive than N'_{SPH} gas particles. Note that this selection criterion (which picks out only rather massive galaxies) is very different from that considered by Benson et al. (2000a) and, as a result, the correlation functions plotted in Fig. 13 are quite different from those in Benson et al. (2000a). Note also that the relatively small volume of the simulations affects the determination of the correlation function for pair separations greater than a few Mpc. To compute the correlation function in the SDSA

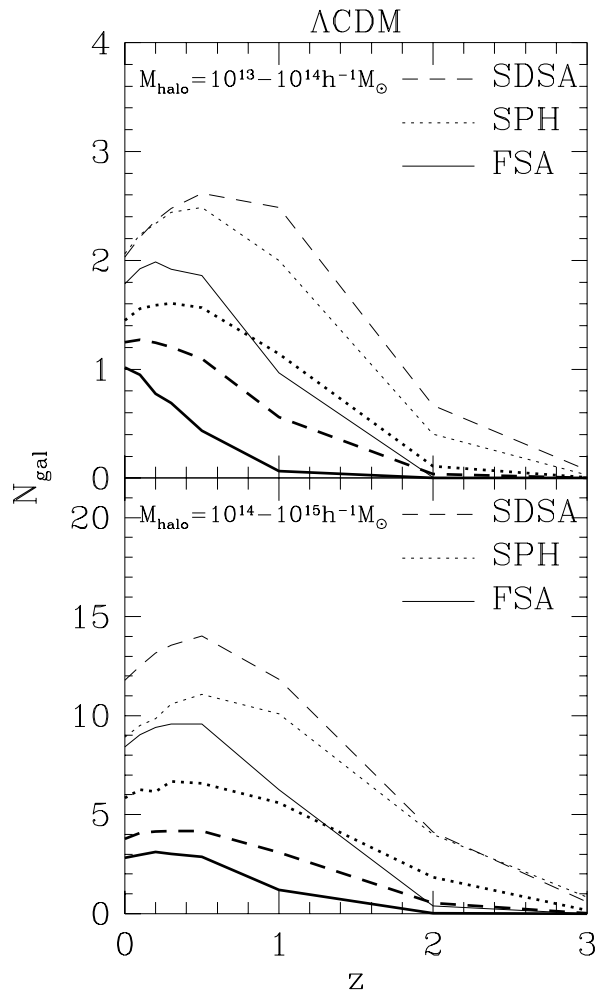


Figure 11. The mean number of progenitor galaxies with mass greater than 64 SPH particles (thin lines) and 128 particles (heavy lines) in the Λ CDM cosmology, as a function of redshift, for halos of present-day mass 10^{13} – $10^{14}h^{-1}M_{\odot}$ (upper panel) and 10^{14} – $10^{15}h^{-1}M_{\odot}$ (lower panel). Dashed, dotted and solid lines show results from the SDSA, SPH and FSA models respectively.

and FSA models, we make the further assumption that the galaxies trace the mass within each dark matter halo.

The agreement of the correlation functions of all three models in both cosmologies is very good, except on scales below $1h^{-1}\text{Mpc}$ in the SCDM cosmology, where the semi-analytic models have a lower amplitude than the SPH simulation. The good agreement is not completely unexpected as the mean number of galaxies per halo is similar in all models, but it does demonstrate that the assumption that galaxies trace the mass within individual halos is a reasonable approximation, at least for studies of the galaxy correlation function. In particular, all the models predict very similar evolution in the correlation function, with galaxies becoming strongly biased at high redshifts.

In Fig. 14 we show the effects of reducing the merger timescale in the Λ CDM cosmology on the galaxy two-point correlation function. The enhanced merger rate significantly lowers the SDSA correlation function below that of the SPH model. Enhancing the cooling rate of gas (by using a fixed

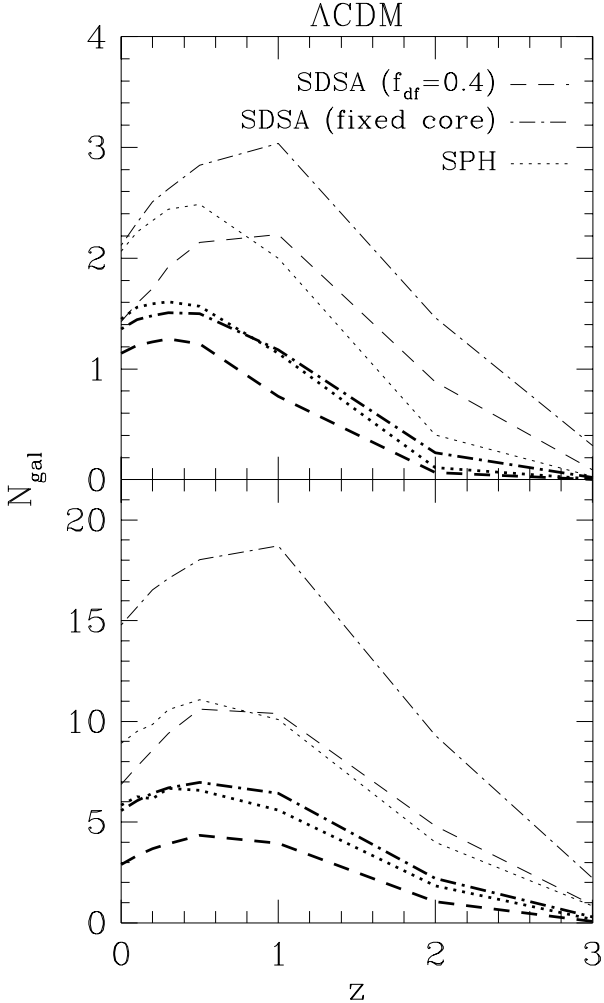


Figure 12. The mean number of progenitor galaxies with mass greater than 64 SPH particles (thin lines) and 128 particles (heavy lines), as a function of redshift in halos of present-day mass 10^{13} – $10^{14} h^{-1} M_{\odot}$ (upper panel) and 10^{14} – $10^{15} h^{-1} M_{\odot}$ (lower panel) in the Λ CDM cosmology. The predictions of the SDSA model are shown in the cases where (i) a faster merger rate is used (dashed line) and (ii) the cooling rate is enhanced by keeping the core radius fixed in the hot gas density profile (dot-dashed line). The dotted line shows the results from the SPH simulation.

gas core radius) in the SDSA model has a negligible effect on the correlation function. This is further evidence that the main difference between the SDSA and SPH models is not a gross difference in galaxy merger rates, but rather a difference in the efficiency with which gas cools.

4 DISCUSSION AND CONCLUSIONS

In this paper we have explored the consistency of two very different techniques commonly used to study galaxy formation, semi-analytic modelling and SPH simulations. For this purpose, we constructed a simplified or ‘stripped-down’ semi-analytic model (SDSA), designed to mimic the conditions of the SPH simulations as closely as possible. An

artificial resolution limit, similar to that in our SPH simulations, was imposed on the SDSA model and the standard star formation and feedback prescriptions normally used in semi-analytic modelling were stripped out. Furthermore, the dark matter halo mass function proposed by Sheth, Mo & Tormen (1999) was used in the SDSA model instead of the standard Press-Schechter formula since the former provides a better match to the mass function in N-body simulations. Similarly, we also modified the extended Press-Schechter theory in order to better match the distribution of progenitor halo masses obtained in the SPH simulations. In this way, we minimize differences in the evolution of dark matter halos and concentrate on the aspect of interest in this work: the evolution of the gas. In this paper, we have focussed on a *statistical* analysis of the differences between the SDSA and SPH models. As a secondary aim, we have also compared the outcome of the SPH simulations with a full semi-analytic model, in which the star formation and feedback prescriptions are restored and no artificial resolution limit is imposed. The motivation for this latter comparison is a desire to assess how the realism of a typical SPH simulation is likely to be compromised by the neglect, or very rough treatment, of star formation and feedback.

For our main comparisons, we considered five properties of the gas distribution in two versions of the CDM cosmology (SCDM and Λ CDM), over the redshift range 0 to 2. In order of decreasing generality, these are: (i) the global fractions of gas in three distinct phases — hot halo, galactic (i.e. cold and dense gas) and uncollapsed; (ii) the amount of cold galactic gas in halos of different mass; (iii) the abundance of objects as a function of their cold gas mass; (iv) the number of ‘galaxies’ as a function of halo mass; and (v) the correlation function of galaxies. The main conclusion of this paper is that the agreement between the SPH simulation and the stripped-down version of the semi-analytic model is better than a pessimist might have expected. The tests we have carried out generally show reasonable agreement between the two techniques, although we have found significant differences in the cold gas mass functions in the two models. Since in both approaches the gas physics are necessarily treated in an approximate fashion, it seems inappropriate to regard one as ‘correct’ and the other as ‘wrong,’ in the instances where discrepancies arise.

Specifically, our main results may be summarized as follows:

(i) Over the simulation volume as a whole, the global amounts of gas in the three main phases that develop (hot, cold galactic and uncollapsed) are very similar in the SDSA model and the SPH simulation. From $z = 0.5$ (the redshift by which about half the final amount of galaxy gas has cooled) to the present, the maximum difference is never larger than 25%. Perhaps surprisingly, the SDSA model produces slightly *less* hot gas than the SPH simulation at all epochs (although this difference may not be significant given the uncertainties inherent in this comparison). The distribution of cold gas in halos of different mass also agrees quite well (to within $\sim 50\%$) with the largest differences occurring in the most massive halos. These results apply to the SPH and SDSA models in their standard forms, i.e. with parameters chosen independently of this comparison in order to match certain observational constraints. Thus, we conclude that in spite of its various approximations (e.g. spherical

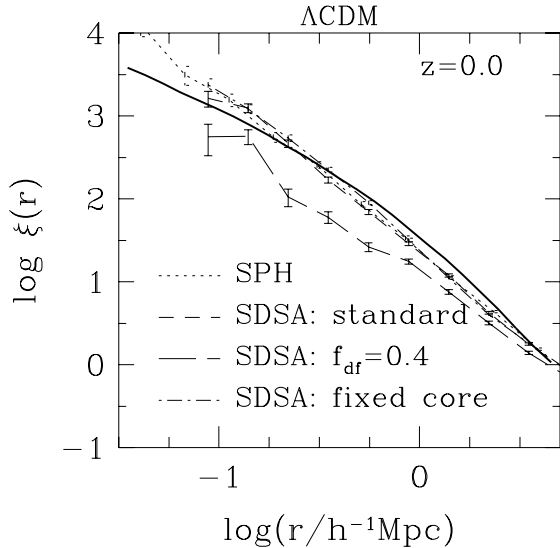


Figure 14. The Λ CDM galaxy two-point correlation function in the SPH and SDSA models at $z = 0$. The SPH model is shown by the dotted line, whilst the standard SDSA model is indicated by the short-dashed line. The long-dashed line shows the SDSA model with an enhanced merger rate ($f_{\text{dr}} = 0.4$), whilst the dot-dashed line shows the SDSA model with a fixed gas core radius. The heavy solid line shows the correlation function of dark matter.

symmetry), the simple model of gas cooling normally employed in semi-analytic models gives similar results, on average, to the SPH simulations.

(ii) Even though the total amount of cold gas is similar in the SDSA model and the SPH simulations, the actual cold gas mass functions (i.e. the abundance of galaxies as a function of cold gas mass) are different, particularly in the Λ CDM cosmology. In this case, the SPH simulation produced three to four times more high-mass galaxies than the SDSA model, or equivalently, at a fixed abundance, galaxies in the SPH simulation are, on average, twice as massive as their SDSA counterparts. We were able to discount a difference in galaxy merging rates as the dominant source of this discrepancy. Instead, we identified as the culprit a difference in the efficiency of cooling in massive galaxies: more gas cools into these galaxies in the SPH simulation than in the standard SDSA model. Thus, artificially increasing the cooling rate of gas in the SDSA model (by assuming that the core radius of the gas density profile remains fixed rather than growing with time as in our standard model) leads to excellent agreement with the SPH galaxy mass functions and also with the mass functions of galaxy progenitors.

(iii) The spatial distribution of galaxies, as characterised by the two-point correlation function, is remarkably similar in the semi-analytic and SPH models. This is true not only of the present-day distribution, but also of the clustering at high redshift. This conclusion also holds even when the cooling rate is enhanced in the SDSA model as discussed in (ii).

The primary limitation of current cosmological SPH simulations is the relatively poor resolution attainable even with the largest computers. By comparing our SPH or SDSA models to the full semi-analytic model (FSA), we gain some

idea of how important these resolution effects are in practice. Furthermore, since the FSA model includes prescriptions for star formation and feedback that are not modelled at all in the SPH simulations we have considered, we can also assess how important these processes are in determining the properties of hot and cold gas in the moderately large galaxies that form in our SPH simulations. The total amount of gas that can cool in an SPH simulation is determined by the resolution limit. On the other hand, because of its intrinsically high resolution, the semi-analytic model traces the evolution of gas even in small halos which the SPH simulation assigns to the uncollapsed phase. As a result, not only is the fraction of halo gas (hot and cold) larger in the FSA model than in the SPH simulation, but its cold gas mass function extends to smaller masses that can be resolved in the SPH simulation. The FSA cold gas mass function has a much sharper cut-off at the massive end than either the SDSA or SPH models.

In summary, our comparisons demonstrate a higher level of consistency than was perhaps expected between the results of SPH simulations and the more idealized semi-analytic models. A particularly uncertain component of the semi-analytic treatment is the assumption that gas cools from a quasi-equilibrium state established when the gas is shock-heated to the virial temperature of a halo during collapse. Our comparisons do not test this assumption directly, only its net effect on the amount of gas that cools. Globally, this turns out to be very similar to the SPH result. However, the semi-analytic model tends to produce somewhat less cool gas in massive halos than the SPH simulation, particularly in the Λ CDM cosmology. We stress that due to the limited resolution of our SPH simulations, our conclusions are restricted to massive galaxies, with baryonic mass of $\gtrsim 10^{11} M_{\odot}$. It will be important to check whether our results still hold in higher resolution simulations. In this paper we have focussed on statistical properties of the galaxy population. Agreement at this level does not necessarily imply agreement on the properties of galaxies on a case-by-case basis. We intend to examine this question in future work. Our present results, however, provide useful support for the reliability of current techniques for modelling galaxy formation in a cosmological context.

ACKNOWLEDGEMENTS

AJB and CSF acknowledge receipt of a PPARC Studentship and Senior Fellowship respectively. CSF also acknowledges receipt of a Leverhulme Research Fellowship. This work was supported in part by a PPARC rolling grant and by the European Community's TMR Network for Galaxy Formation and Evolution. We acknowledge the Virgo Consortium for making available the simulations used in this study and our colleagues, Shaun Cole and Cedric Lacey, for allowing us to use results from the Durham semi-analytic galaxy formation model. We are grateful to Shaun Cole and David Weinberg for many stimulating discussions, and to James Binney whose incisive questions encouraged us to pursue this project. These simulations were carried out on the T3D at the Edinburgh Parallel Computing Centre (EPCC).

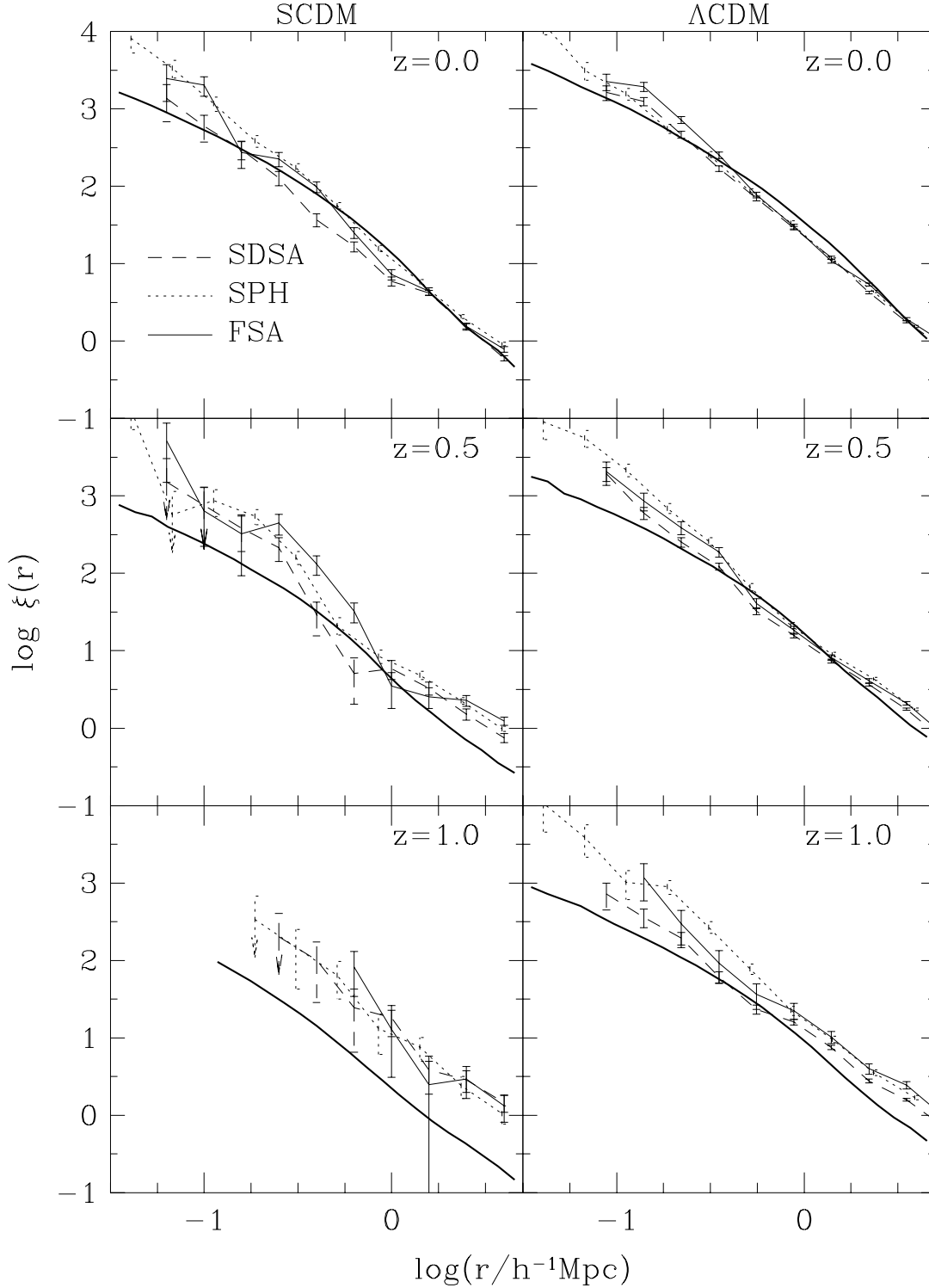


Figure 13. Two-point galaxy correlation functions from the SPH, FSA and SDSA models are shown as the dotted, solid and dashed lines respectively. The thick solid line shows the correlation function of dark matter in the simulations. Galaxies from all the models are chosen to have a mass in cold gas plus stars greater than 64 times the SPH gas particle mass. SCDM and Λ CDM cosmologies are shown in left and right-hand panels respectively. Results are shown at $z = 0, 0.5$ and 1 as indicated in each panel. Downwards-pointing arrows are used where the lower errorbar drops below zero.

REFERENCES

Baugh C. M., Cole S., Frenk C. S., 1996a, MNRAS, 282, L27
 Baugh C. M., Cole S., Frenk C. S., 1996b, MNRAS, 283, 1361
 Baugh C. M., Cole S., Frenk C. S., Lacey C. G., 1998, ApJ, 498, 504
 Baugh C. M., Benson A. J., Cole S., Frenk C. S., Lacey C. G., 1999, MNRAS, 305, L21
 Benson A. J., Cole S., Frenk C. S., Baugh C. M., Lacey C. G., 2000a, MNRAS, 311, 793
 Benson A. J., Baugh C. M., Cole S., Frenk C. S., Lacey C. G., 2000b, MNRAS, 316, 107
 Binney J. J., 1977, ApJ, 215, 483
 Bond J. R., Kaiser N., Cole S., Efstathiou G., 1991, ApJ, 379, 440
 Bower R.G., 1991, MNRAS, 248, 332
 Cole, S., 1991, ApJ, 367, 45
 Cole, S., Aragon-Salamanca A., Frenk C. S., Navarro J.F., Zepf S. E., 1994, MNRAS, 271, 781
 Cole S., Lacey C. G., Baugh C. M., Frenk C. S., 2000, MNRAS in press
 Colín P., Klypin A., Kravtsov A., Khokhlov A., 1999, ApJ, 523, 32
 Colpi M., Mayer L., Governato F., 1999, ApJ, 525, 720
 Copi C. J., Schramm D. N., Turner M. S., 1995, ApJ, 455, L95
 Davis M., Efstathiou G., Frenk C.S. & White S.D.M., 1985, ApJ, 292, 371
 Diaferio A., Kauffmann G., Colberg J. M., White S. D. M., 1999, MNRAS, 307, 537
 Eke V. R., Cole S., Frenk C. S., 1996, MNRAS, 282, 263
 Eke V. R., Navarro J. F., Frenk C. S., 1998, ApJ, 503, 569
 Evrard A. E., Summers F. J., Davis M., 1994, ApJ, 422, 11
 Frenk C. S., Evrard A. E., White S. D. M., Summers F. J., 1996, ApJ, 472, 460
 Frenk et al., 1999, ApJ, 525, 554
 Gingold R.A., Monaghan J.J., 1977, MNRAS, 181, 375
 Governato F., Baugh C. M., Frenk C. S., Cole S., Lacey C. G., Quinn T., Stadel J., 1998, Nat, 392,359
 Jenkins A., Frenk C. S., Pearce F. R., Thomas P., Colberg J., White S. D. M., Couchman H., Peacock J., Efstathiou G., Nelson A. (the VIRGO Consortium), 1998, ApJ, 499, 20
 Jenkins A., Frenk C. S., White, S. D. M., Colberg, J. M., Cole S., Evrard A. E., Yoshida N., 2000, submitted to MNRAS, (astro-ph/0005260)
 Katz N., Gunn J. E., 1991, ApJ, 377, 365
 Katz N., Hernquist L., Weinberg D. H., 1992, ApJ, 399, L109
 Katz N., Weinberg D. H., Hernquist L., 1996, ApJS, 105, 19
 Kauffmann G., White, S. D. M., Guiderdoni, B., 1993, MNRAS, 264, 201
 Kauffmann G., Guiderdoni, B., White, S. D. M., 1994, MNRAS, 267, 981
 Kauffmann G., 1995, MNRAS, 274, 153
 Kauffmann G., 1996a, MNRAS, 281, 475
 Kauffmann G., 1996b, MNRAS, 281, 487
 Kauffmann G., Charlot S., 1998a, MNRAS, 294, 705
 Kauffmann G., Charlot S., 1998b, MNRAS, 297, 23
 Kauffmann G., Nusser A., Steinmetz M., 1997, MNRAS, 286, 795
 Kauffmann G., Colberg J. M., Diaferio A., White S. D. M., 1999a, MNRAS, 303, 188
 Kauffmann G., Colberg J. M., Diaferio A., White S. D. M., 1999b, MNRAS, 307, 529
 Kay S. T., Pearce F. R., Jenkins A., Frenk C. S., White S. D. M., Thomas P. A., Couchman H. M. P., 2000, MNRAS, 316, 374
 Lacey C. G., Silk J., 1991, ApJ, 381, 14
 Lacey C. G., Guiderdoni B., Rocca-Volmerange B., Silk J., 1993, ApJ, 402, 15.
 Lacey C. G., Cole S., 1993, MNRAS, 262, 627
 Lacey C. G., Cole S., 1994, MNRAS, 271, 676
 Lucy L., 1977, AJ, 82, 1013
 Monaghan, J. J. 1992, ARA&A, 30, 543
 Navarro J. F., White S. D. M., 1993, MNRAS, 265, 271
 Navarro J. F., Frenk C. S., White S. D. M., 1995, MNRAS, 275, 720
 Navarro J. F., Frenk C. S., White S. D. M., 1996, ApJ, 462, 563
 Navarro J. F., Frenk C. S., White S. D. M., 1997, ApJ, 490, 493
 Navarro J. F., Steinmetz M., 1999, ApJ, 513, 555
 Pearce F. R., Couchman H. M. P., 1997, New Astronomy, 2, 411
 Pearce F. R., Jenkins A., Frenk C. S., Colberg J. M., White S. D. M., Thomas P. A., Couchman H. M. P., Peacock J. A., Efstathiou G. (The VIRGO Consortium), 1999, ApJ, 521, 99
 Pearce F. R. et al., 2000, in preparation
 Press W. H., Schechter P., 1974, ApJ, 187, 425
 Raymond J. C., Cox D. P., Smith B. W., 1976, ApJ, 204, 290
 Ritchie B. W., Thomas P. A., 2000, astro-ph/0005357 (submitted to MNRAS)
 Rees M. J., Ostriker J. P., 1977, MNRAS, 179, 541
 Sheth R. K., Tormen G., 1999, MNRAS, 308, 119.
 Sheth R. K., Mo H. J., Tormen G., 1999, submitted to MNRAS (astro-ph/99070204)
 Silk J., 1977, ApJ, 211, 638
 Somerville R. S., Primack J. R., 1999, MNRAS, 310, 1087
 Somerville R.S., Lemson G., Kolatt T.S., Dekel A., 2000, MNRAS, 316, 479
 Steinmetz M., Müller E., 1994, A&A, 281, 97
 Steinmetz M., Müller E., 1995, MNRAS, 276, 549
 Sutherland R. S., Dopita M. A., 1993, ApJS, 88, 253
 Thacker R. J., Tittley E. R., Pearce F. R., Couchman H. M. P., Thomas P. A., 1998, astro-ph/9809221
 Tittley E. R., Couchman H. M. P., Pearce F. R., 1999, astro-ph/9911017 (submitted to MNRAS)
 Tormen G., 1997, MNRAS, 290, 411
 Tormen G., 1998, MNRAS, 297, 648
 Weil M. L., Eke V. R., Efstathiou, G., 1998, MNRAS, 300, 773
 White S. D. M., Frenk C. S., 1991, ApJ, 379, 52
 White S. D. M., Rees M. J., 1978, MNRAS, 183, 341